ESI

Table of Contents

I. Materials

Fmoc-Ala-OH, Fmoc-Phenylalanine, Pyren-1-ylmethanamine hydrochloride , [2,2'-Bipyridine]-3,3'-dicarboxylic acid, 2-iodobiphenyl, and 3-chloroperoxybenzoic acid (m-CPBA) were purchased from Shanghai Bide Medical Technology Co., LTD. Trifluoromethanesulfonic acid (TfOH) and sodium tetrakis[3,5-bis(trifluoromethyl)phenyl]borate ($NaBAr^F_4$) were purchased from Shanghai Macklin Biochemical Co., Ltd (China). All solvents were purchased from Jinan Saibo Instrument Co., Ltd. All chemicals were used without further purification.

II. Instrumentation

Nuclear magnetic resonance (NMR) spectra were obtained using Bruker AM-400 spectrometer at room temperature with tetramethylsilane (TMS) as the reference. **High resolution mass (HRMS)** spectra were collected with an Ultra-performance liquid chromatography coupled to quadrupole Tine-of-flight spectrometer (Bruker, impact II), the charging voltage and dry heater temperature were set at 2000 V and 180 ^oC respectively. **Fluorescence quantum yield and life time** were recorded *via* FLS-1000 photoluminescence spectrometer from Edinburgh Instruments Ltd. (UK). **Circular dichroism (CD)** spectra were measured with an Applied Photophysics Chirascan V100

model (UK). **Circularly polarized luminescence (CPL)** were acquired by JASCO CPL 300. **UV-vis absorption spectra** were collected with the Shimadzu RF-6000 spectrophotometer (Japan). **Fluorescence spectra** were obtained at room temperature using Shimadzu RF6000 spectrometer. **FT-IR spectra** were measured with a Bruker Tensor II spectrometer, the resolution is 0.4 cm^{-1}. **Powder X-ray diffraction (XRD) patterns** were collected on a PANalytical (X'Pert3 Powder&XRK-900) X-ray diffraction (UK) with Cu Kα radiation (λ = 0.15406 nm, voltage 45 KV, current 200 mA, power 9 KW). **Scanning Electron Microscope (SEM)** images were obtained by a G500 FE-SEM System. **X-ray photoelectron spectroscopy (XPS)** measurements were performed on a Thermo Fisher-VG Scientific (ESCALAB 250Xi) photoelectron spectrometer equipped with a monochromatic Al Kα X-ray source (hν = 1486.8 eV). The sample was loaded into a custom built air-free sample holder, under a N_2 atmosphere. Prior to data collection, a baseline vacuum of 1.07×10^{-9} mbar was achieved. For high resolution scans, a band pass energy of 30 eV was used. Binding energies were calibrated using the C1s peak of adventitious carbon at 284.8 eV. **Grazing incidence wide-angle X-ray scattering (GIWAXS)** measurements were conducted at a Xeuss 3.0 SAXS/WAXS laboratory beamline at Vacuum Interconnected Nanotech Workstation (Nano-X) in China with Kα X-ray of Cu source (operated at 50kV, 0.06 mA, 1.542 Å). GIWAXS patterns were recorded by a two dimensional X-ray detector (Eiger2 R 1M, Dectris). The incident angle was set to 0.18 degree.

III. Methods

Non-Covalent Interaction (NCI) analysis

The Multiwfn software is used to import the .fchk file and visually analyze weak interactions. Function 20 is employed for studying weak interactions graphically, with subfunction 1 used for normal NCI (Non-Covalent Interaction) analysis. Appropriate grid settings are sequentially selected for calculating these functions. In the current software configuration, output cube files are exported to func1.cub and func2.cub in the current directory. These exported files are then imported and plotted using the VMD

program, resulting in the generation of a RDG (Reduced Density Gradient) iso-surface.

Binding constant calculation

In Origin software, I employed the 1:1 binding model equation (y = P3 - (P1/2) * (P4 + x + 1/P2 - sqrt((P4 + x + 1/P2)^2 - 4 * P4 * x))), where P2 represents the binding constant (Ka) and P4 corresponds to [G_0]. The binding constant was obtained through nonlinear fitting.

Quantum mechanical calculation of ECD spectrum

For compounds, the absolute conformations of monomers in solution were constructed using GaussView 6.0. These structures were subjected to preliminary optimization using the Gaussian 16 program with the B3LYP/DEF2SVP method to obtain low-energy conformations, preserving the original geometric shapes without significant alteration. Then, the same density functional and basis set were employed to compute absorption/ECD spectra using time-dependent density functional theory (TDDFT). The calculation included settings where “nstates” was set to 120, representing information on the 120 excited states with the lowest total computational energy. Additionally, the Solvation Model Based on Density (SMD) was applied as the implicit solvent model, with TCM used as the built-in solvent. Using the Gaussian output file, UV-Vis and ECD spectra can be generated and plotted using GaussView 6.0.

Molecular dynamic (MD) simulation

"We constructed and initially optimized the geometries using the Gaussian View 06 program. The electrostatic potential was calculated via the Hartree-Fock method with the B3LYP/DEF2SVP basis set. To fit the restrained electrostatic potential charges, the Antechamber program was employed, and the General Amber Force Field (GAFF) was utilized for parameterization for subsequent MD simulations. The topology files of the molecule were parameterized under the guidance of the GROMACS force field using Amber, ACPYPE, and Gaussian tools.

The MD simulation of the assembled system proceeded as follows: we created a simulation box of dimensions 10×10×10 nm³ and inserted 200 PAP molecules into the box by free dispersing (PPP as well). The MD simulation was conducted for 15 ns with a time step of 0.0005 ps per step at 298 K. All simulations were performed using the GROMACS 2020 program.

IV. Supplement Data

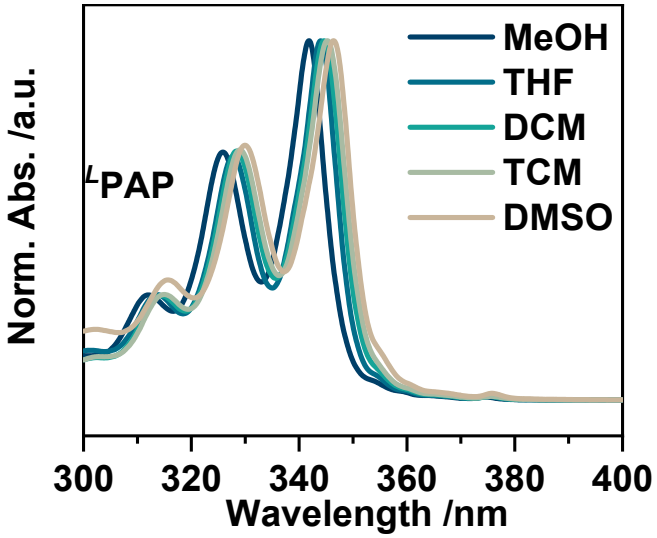

Figure S1: Normalized UV-vis absorption of ^{L}PAP in different solvents.

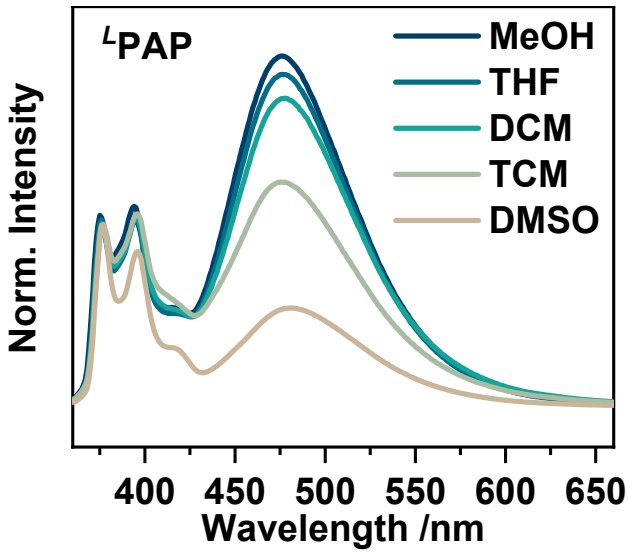

Figure S2: Normalized fluorescence of ^{L}PAP in different solvents.

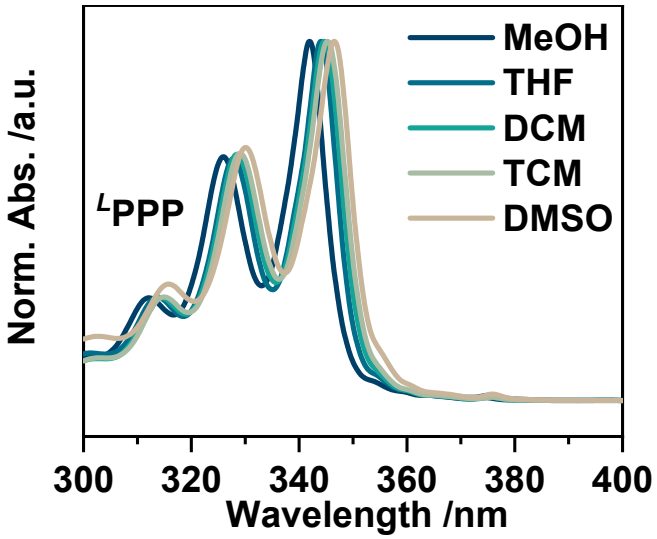

Figure S3: Normalized UV-vis absorption of ^{L}PPP in different solvents.

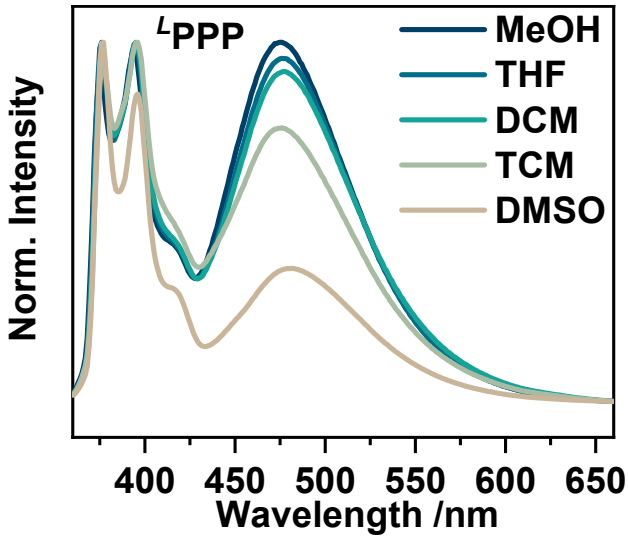

Figure S4: Normalized fluorescence of ^{L}PPP in different solvents.

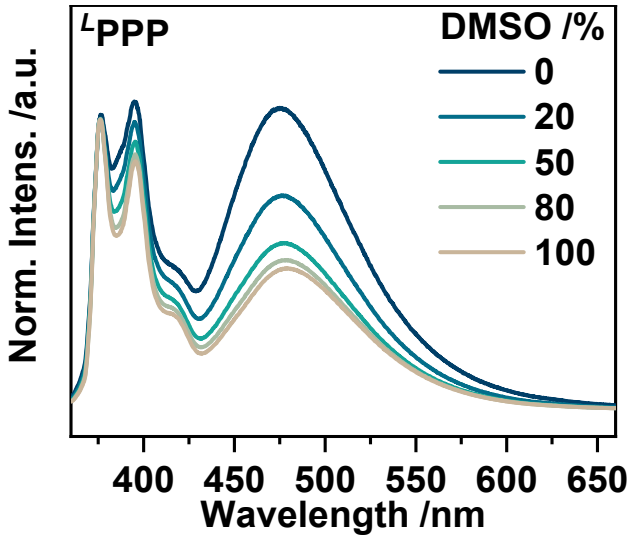

Figure S5: Normalized fluorescence intensity of ^{L}PAP with different DMSO volume fraction (DMSO/TCM).

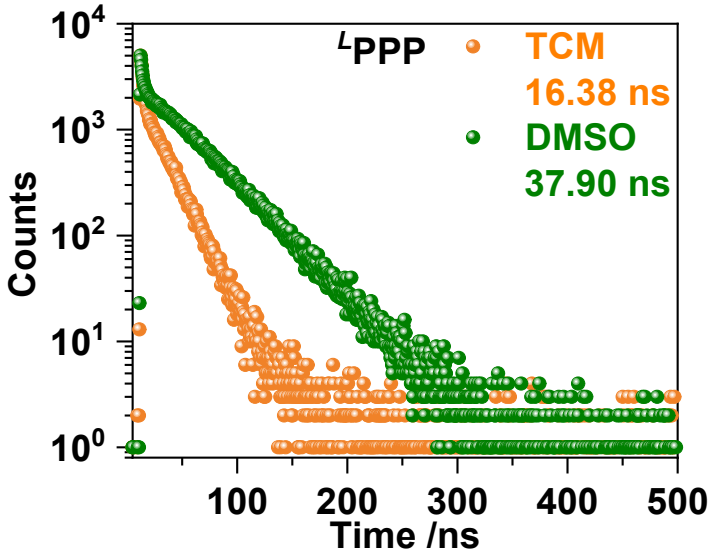

Figure S6: Fluorescence lifetime of ^{L}PPP in TCM and DMSO.

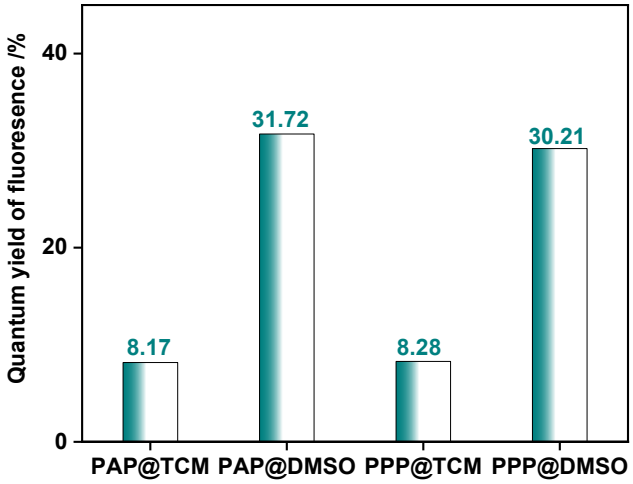

Figure S7: Fluorescence quantum yields of PAP and PPP in TCM and DMSO.

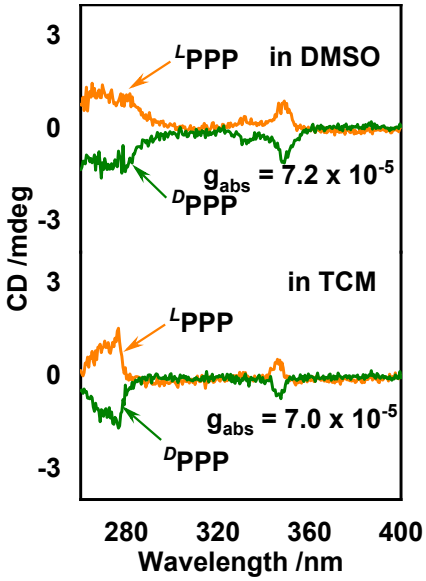

Figure S8: CD spectra of $^{L/D}$PPP in TCM and DMSO.

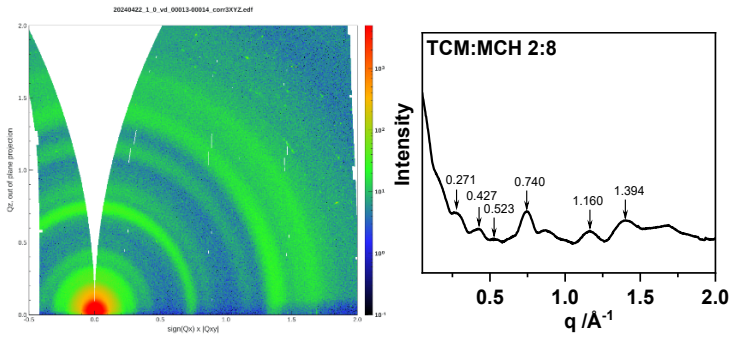

Figure S9: GIXS patterns and corresponding integral peaks for ^{L}PPP (f_{MCH}= 80%)

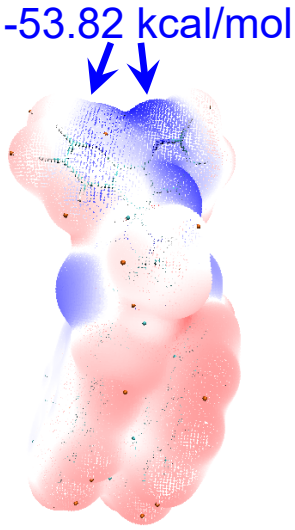

Figure S10: ESP of and ^{L}PAP

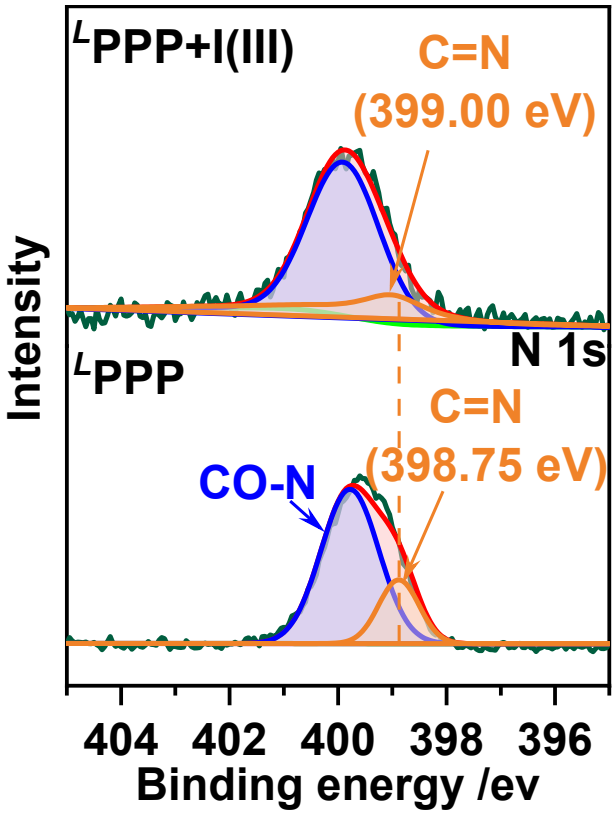

Figure S11: XPS patterns of ^{L}PPP and its halogen bonding complex with the 1:1 ratio.

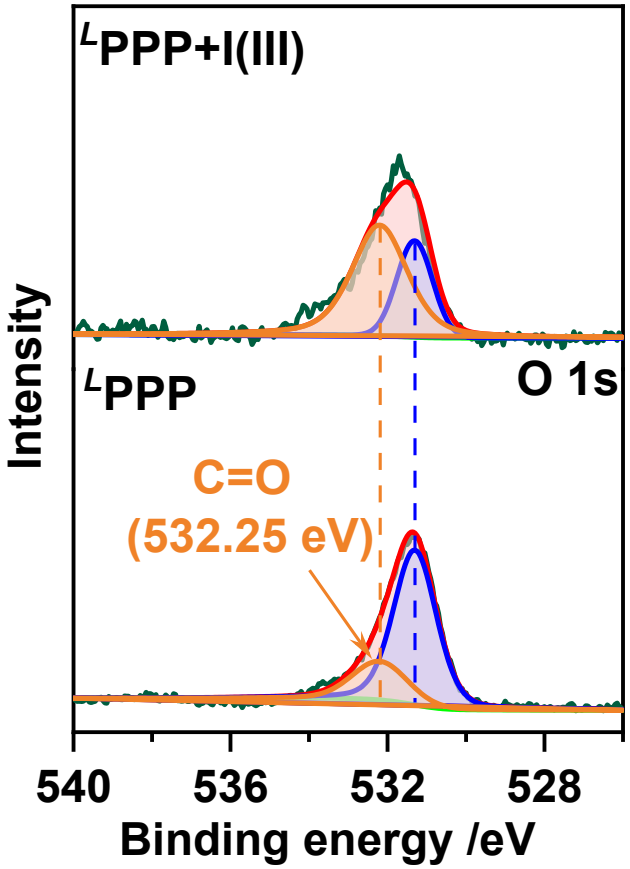

Figure S12: XPS patterns of ^{L}PPP and its halogen bonding complex with the 1:1 ratio.

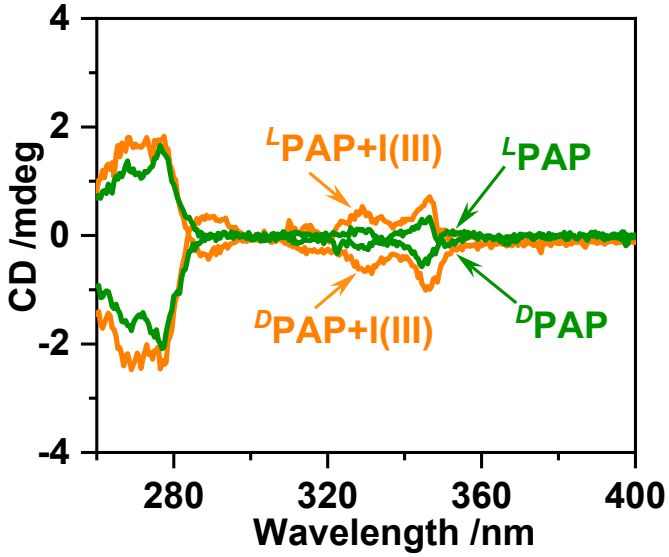

Figure S13: CD spectra of $^{L/D}$PAP and $^{L/D}$PAP with I(III) in TCM.

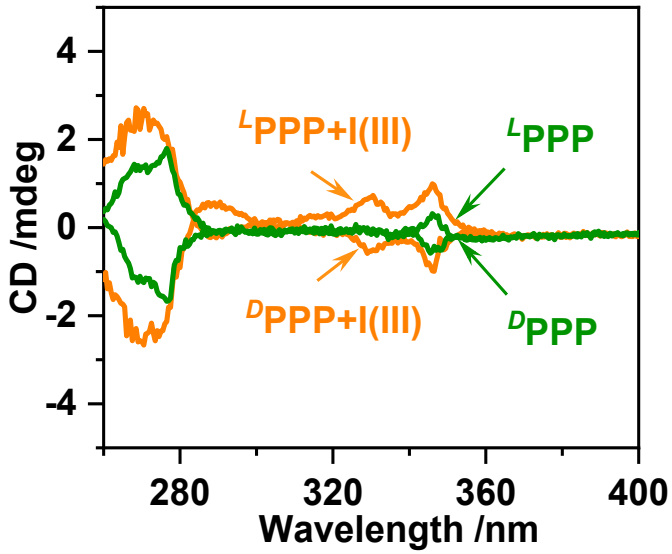

Figure S14: CD spectra of $^{L/D}$PPP and $^{L/D}$PPP with I(III) in TCM.

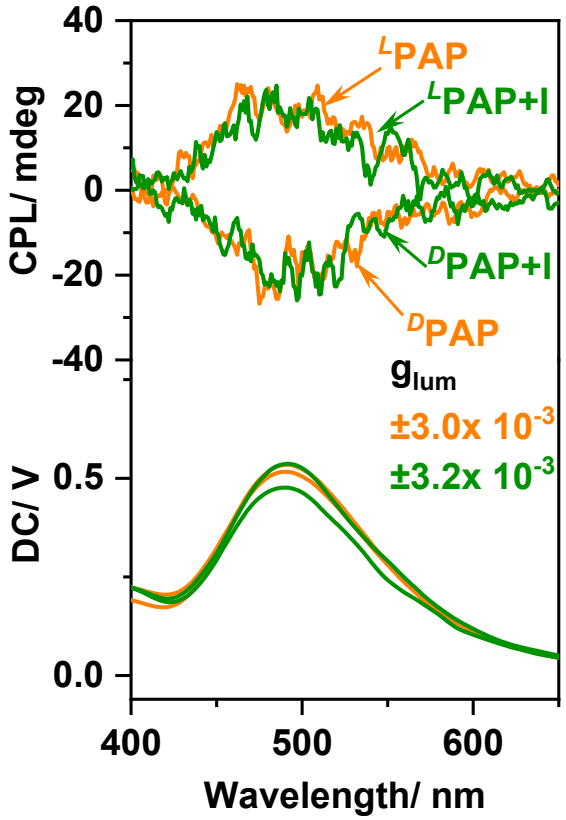

Figure S15: CPL spectra of $^{L/D}$PAP and $^{L/D}$PAP with I(III) in TCM.

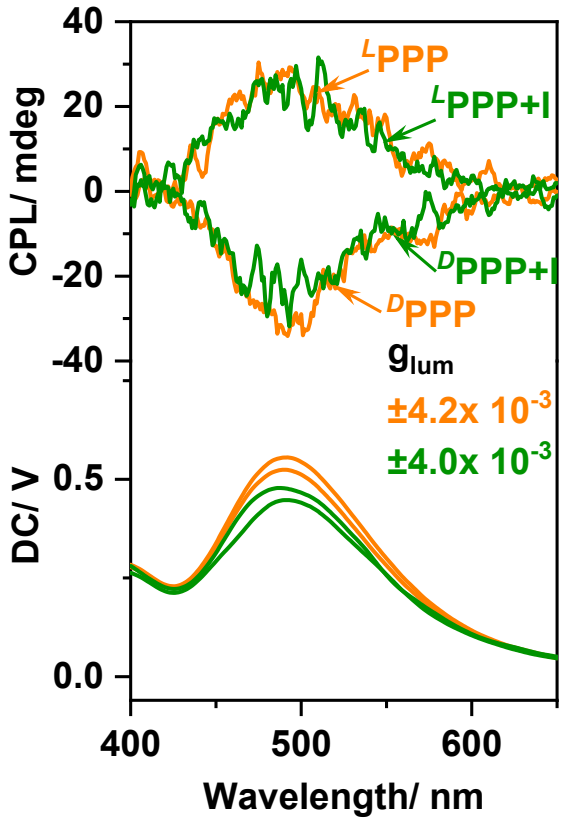

Figure S16: CPL spectra of $^{L/D}$PPP and $^{L/D}$PPP with I(III) in TCM.

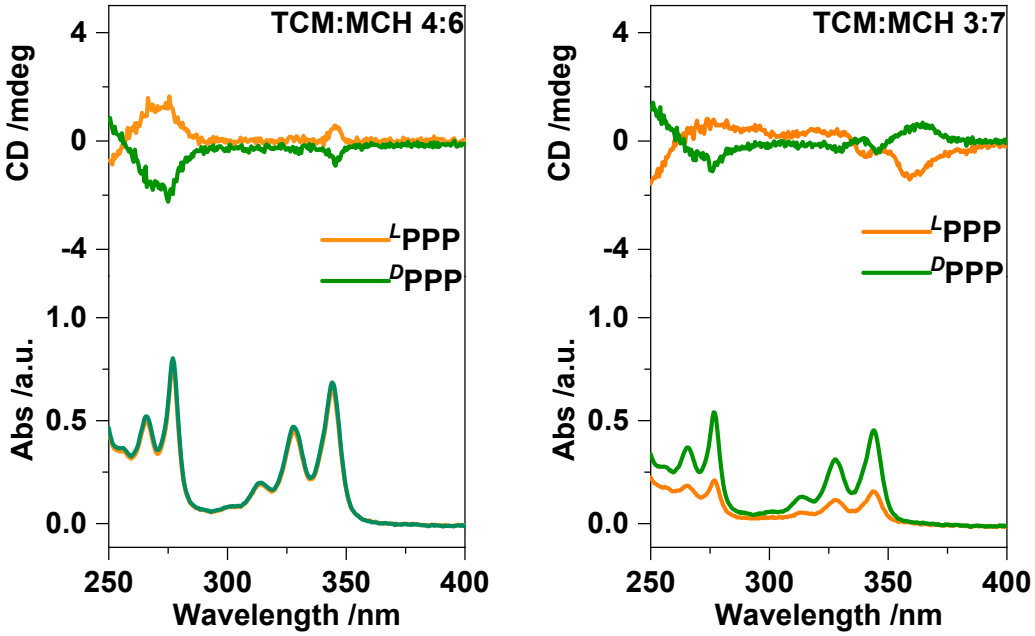

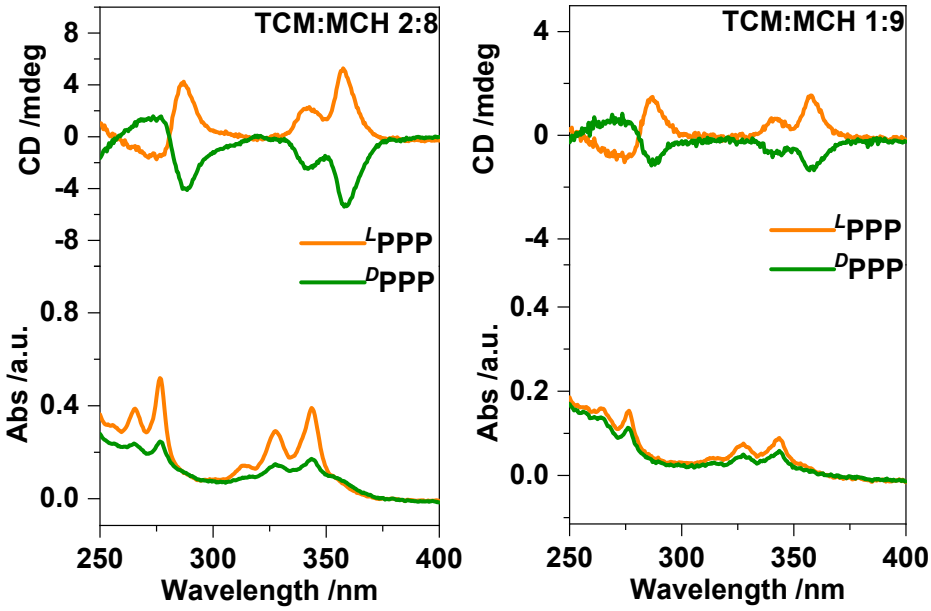

Figure S17: CD spectra of $^{L/D}$PPP in different assembly conditions.

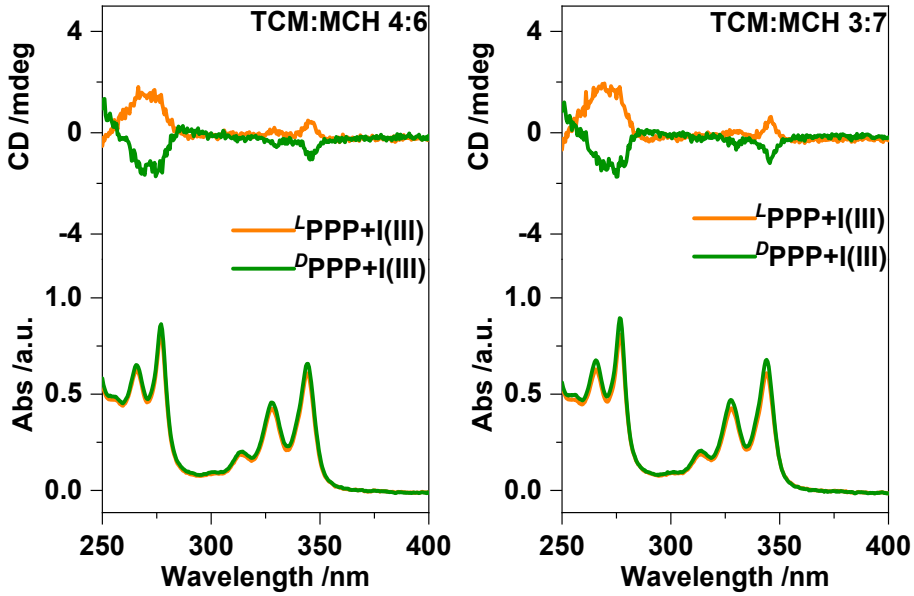

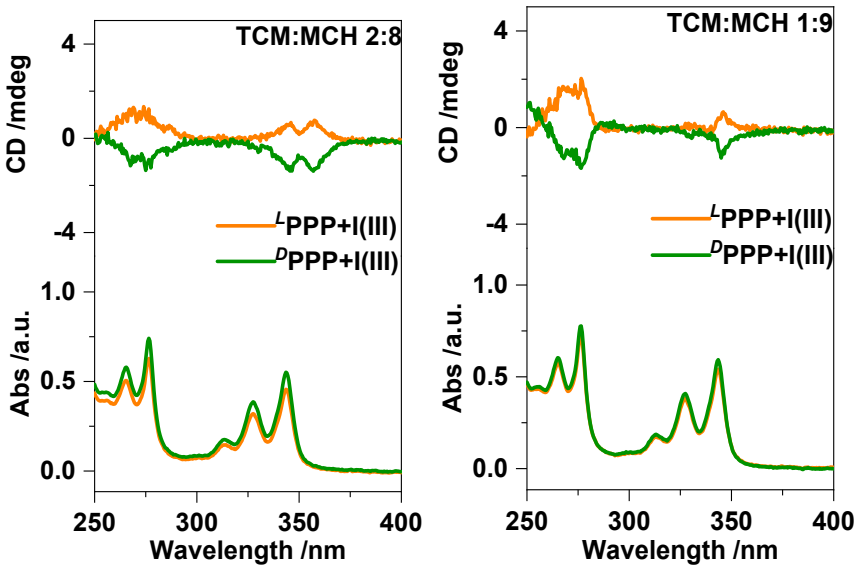

Figure S18: CD spectra of $^{L/D}$PPP with I(III) in different assembly conditions.

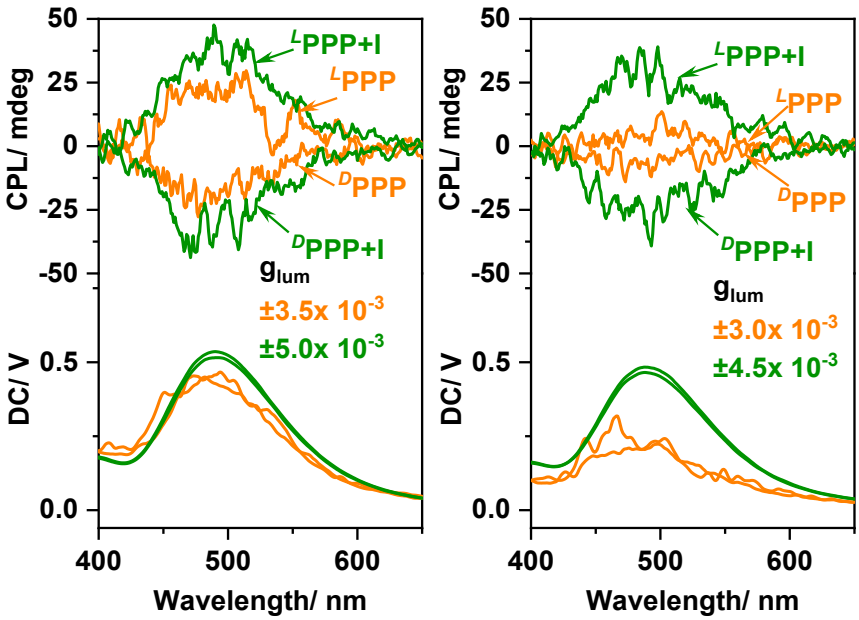

Figure S19: CPL spectra of $^{L/D}$PPP, and $^{L/D}$PPP with I(III) in different assembly conditions, f_{MCH}= 70% and 80%, respectively.

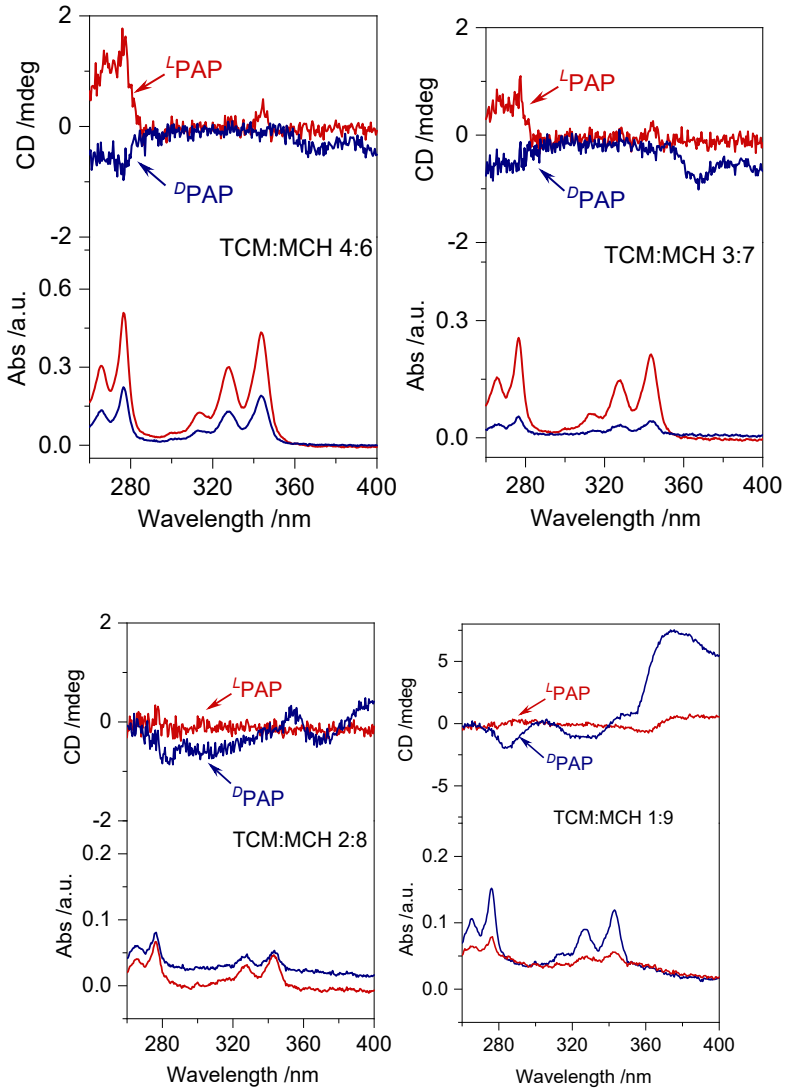

Figure S20: CD spectra of $^{L/D}$PAP in different assembly conditions.

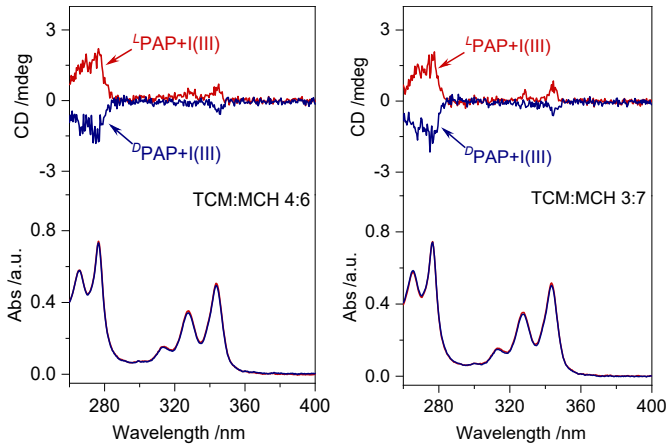

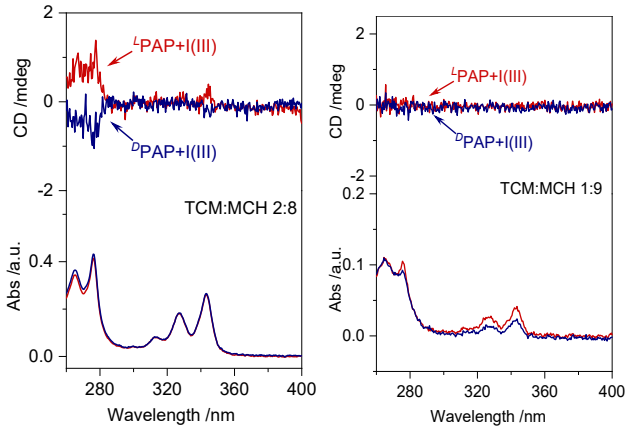

Figure S21: CD spectra of $^{L/D}$PAP+I(III) in different assembly conditions.

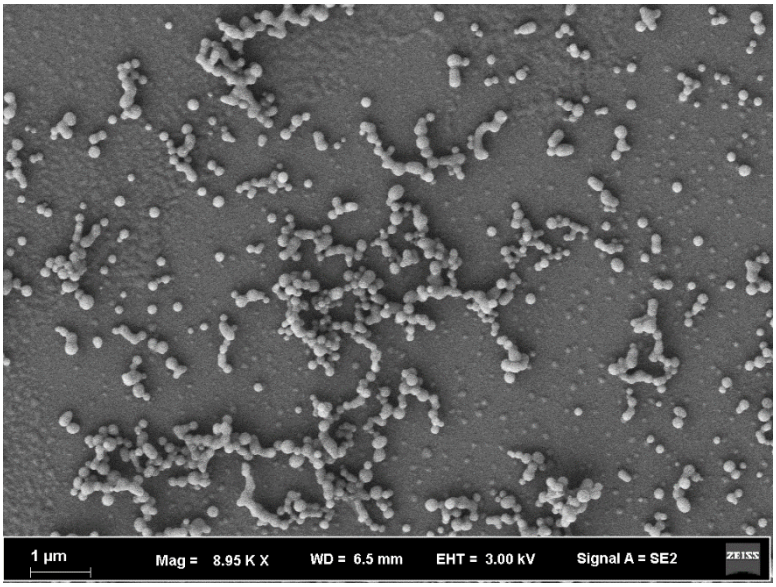

Figure S22: SEM of ^{L}PAP with I(III) in TCM and MCH (f_{MCH}= 60%).

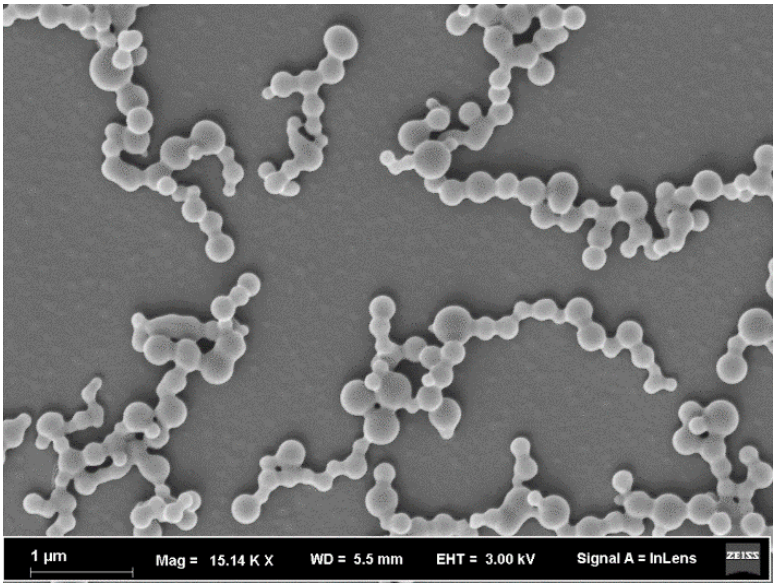

Figure S23: SEM of ^{L}PAP with I(III) in TCM and MCH (f_{MCH}= 70%).

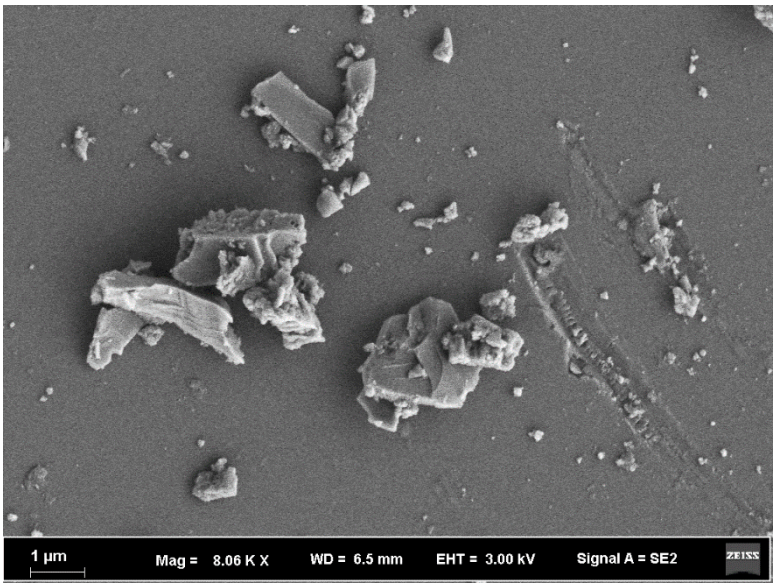

Figure S24: SEM of ^{L}PAP with I(III) in TCM and MCH (f_{MCH}= 80%).

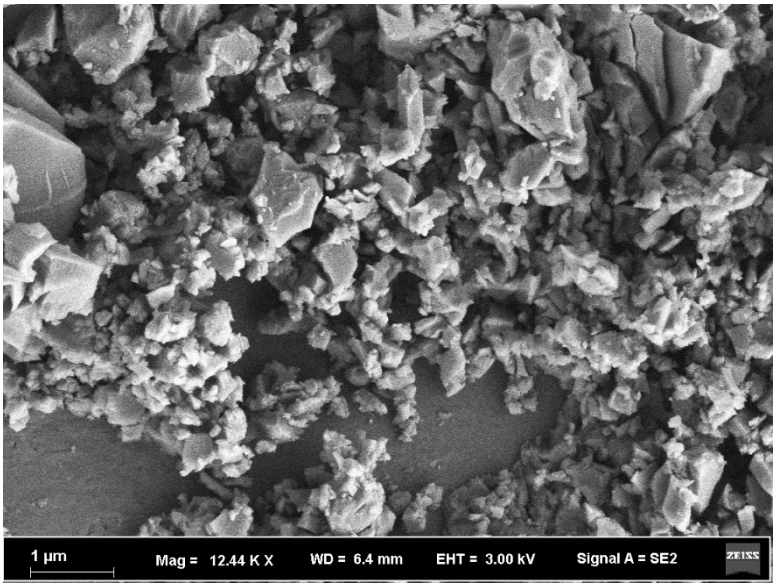

Figure S25: SEM of ^{L}PAP with I(III) in TCM and MCH (f_{MCH}= 90%).

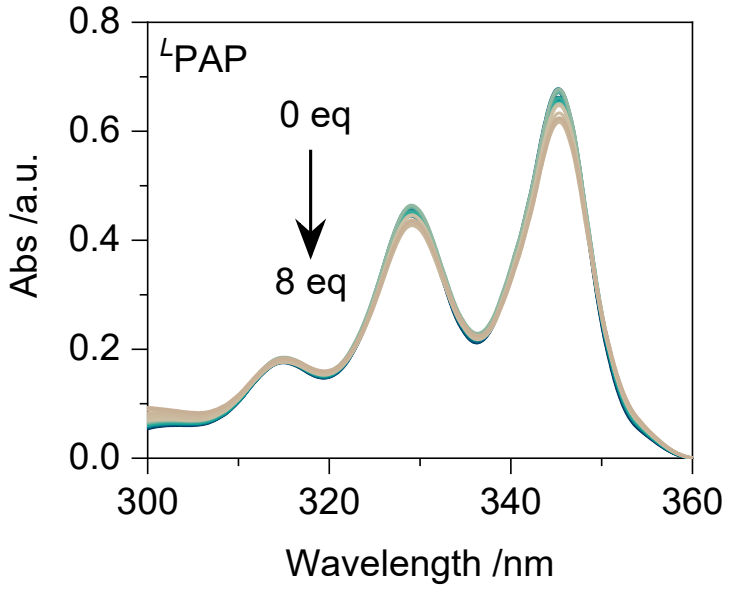

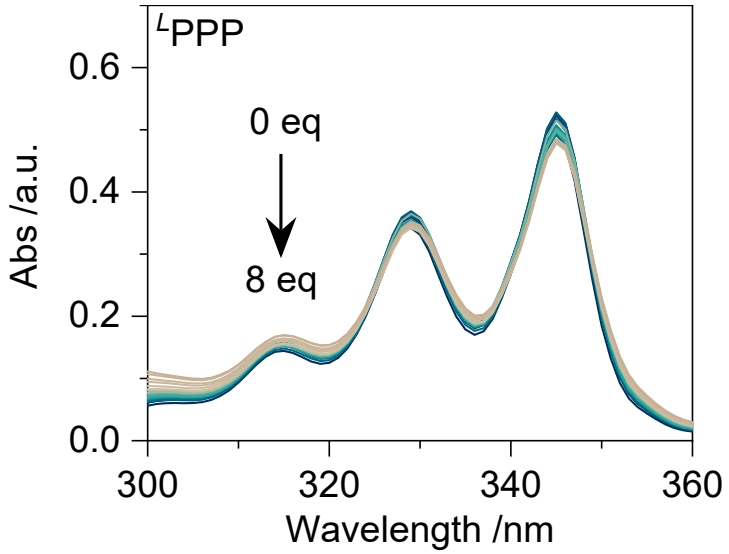

Figure S26: Changes in the UV absorption of PAP and PPP after the addition of different equivalents of I(III).

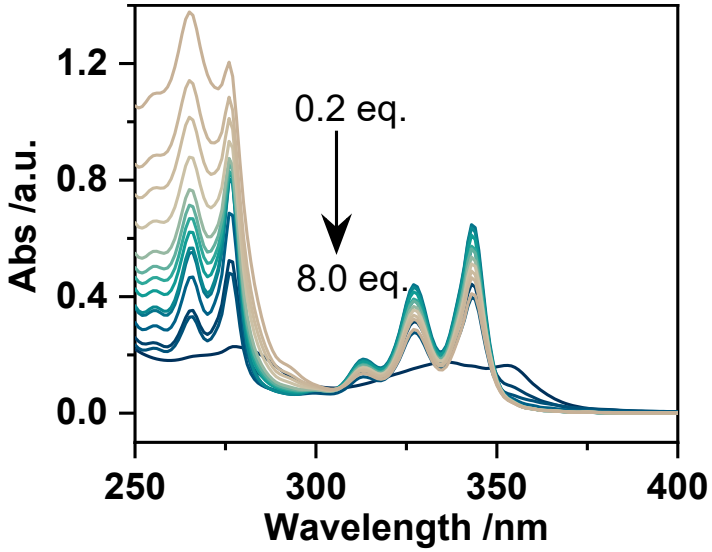

Figure S27: UV-vis absorption experiments of ^{L}PPP in TCM and MCH (1:9) with the addition of I(III).

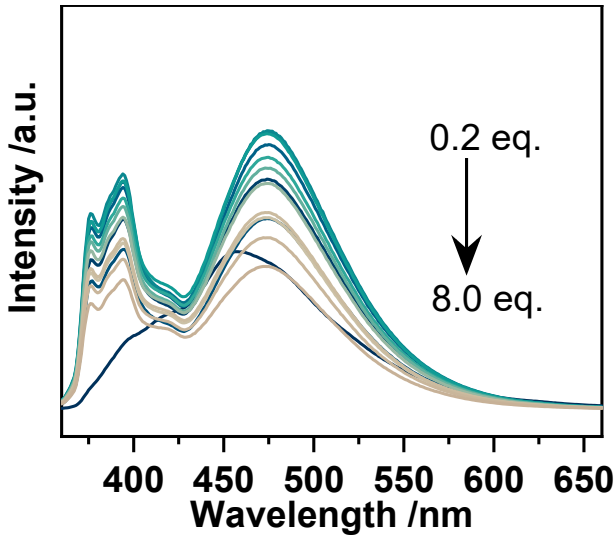

Figure S28: Fluorescence titration experiments of ^{L}PPP in TCM and MCH (1:9) with the addition of I(III).

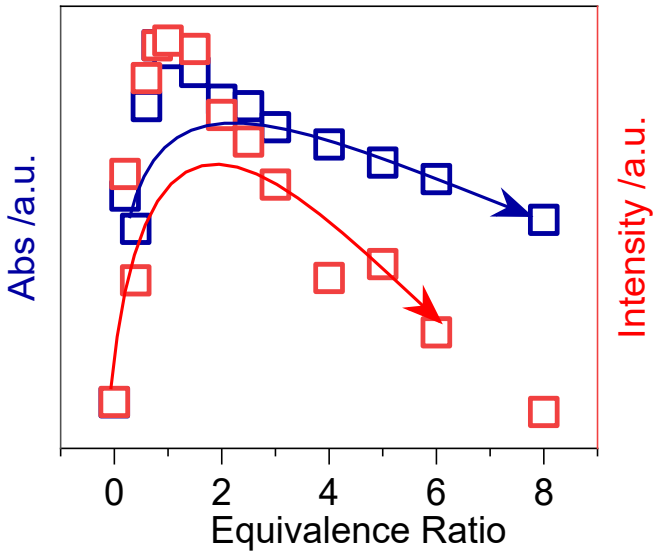

Figure S29: UV absorption of PPP at 343 nm and fluorescence intensity at 476 nm under different equivalents of I(III).

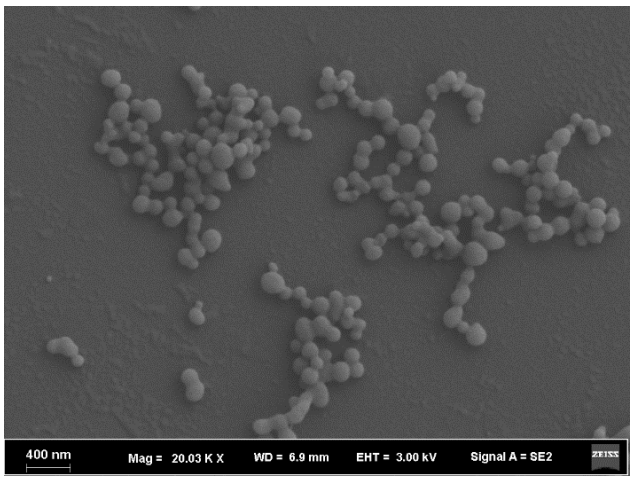

Figure S30: SEM of ^{L}PPP with I(III) in TCM with f_{MCH} = 70%, the concentrations of PPP and I(III) are both 0.02 mM.

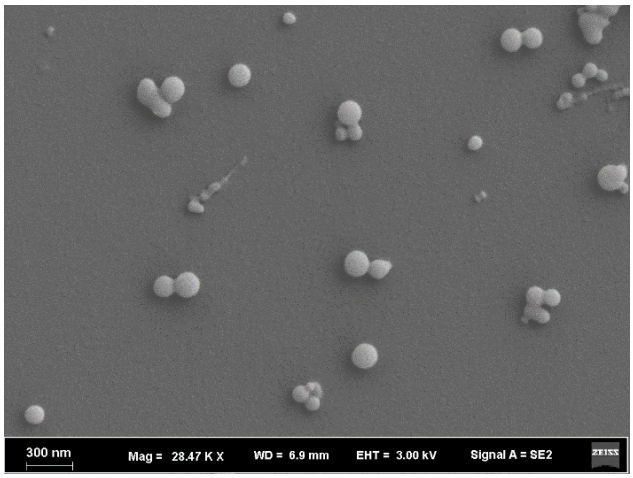

Figure S31: SEM of ^{L}PPP with I(III) in TCM with f_{MCH} = 80%, the concentrations of PPP and I(III) are both 0.02 mM.

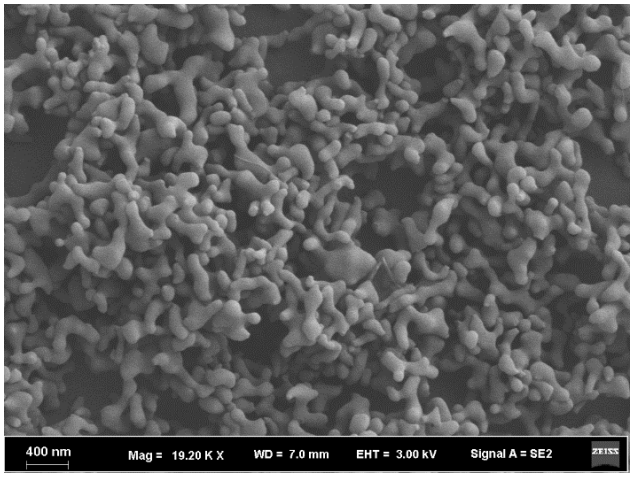

Figure S32: SEM of ^{L}PPP with I(III) in TCM with f_{MCH} = 90%, the concentrations of PPP and I(III) are both 0.02 mM.

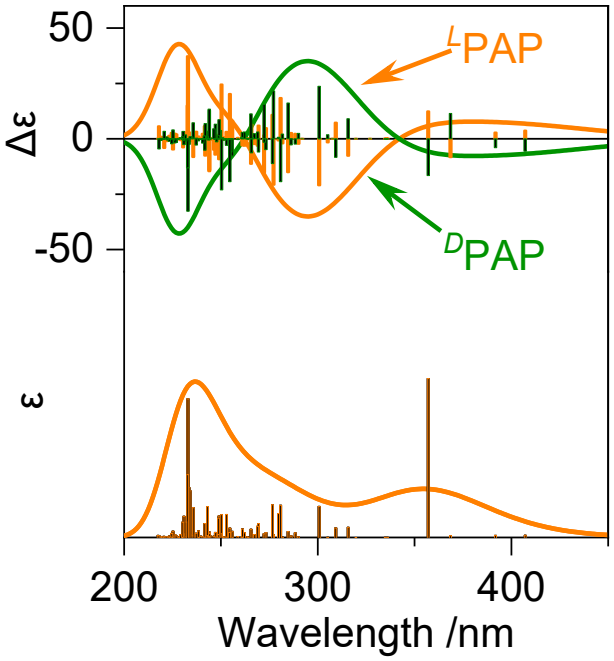

Figure S33: Calculated CD spectra of $^{L/D}$PAP and L/DPPP. In the calculated spectra, the vertical lines indicate the original electric transition states.

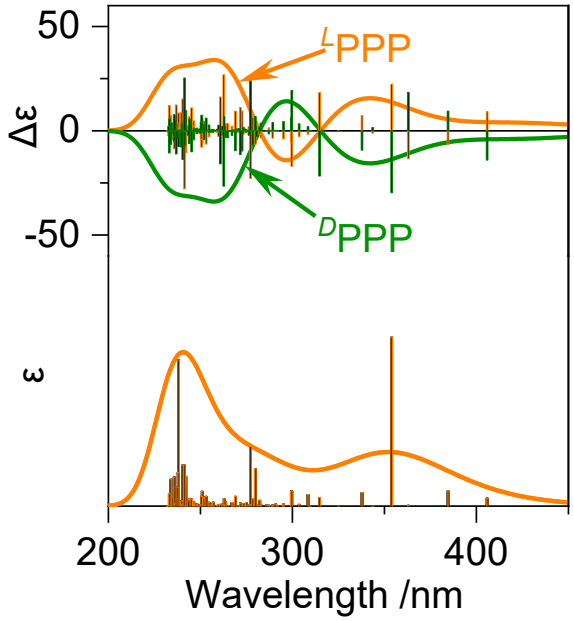

Figure S34: Calculated CD spectra of $^{L/D}$PPP . In the calculated spectra, the vertical lines indicate the original electric transition states.

The electronic circular dichroism (ECD) calculations performed using time-dependent density functional theory (TD-DFT) corroborate the experimental CD findings (Figure S33-S34). Theoretical ECD spectra of ^{L}PPP show prominent peaks at 258 nm and 342 nm, displaying positive signals that closely match the experimental observations.

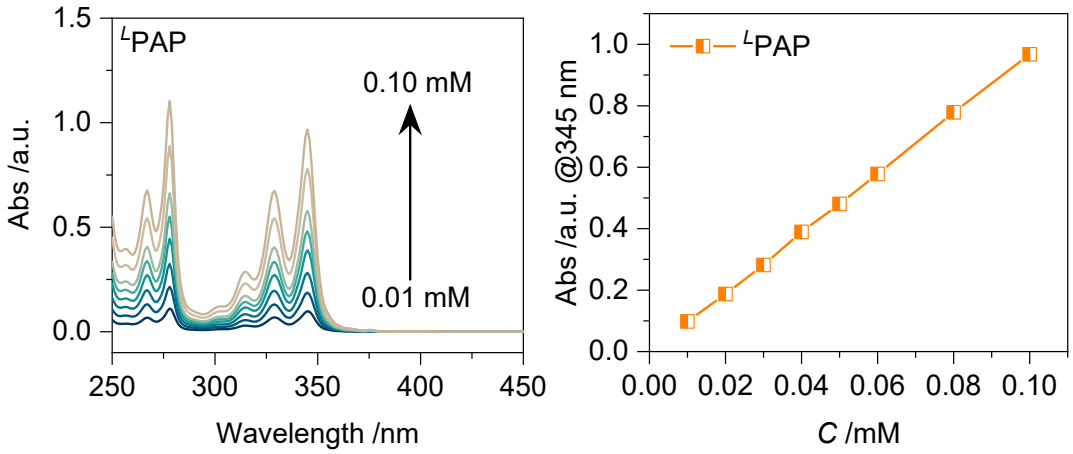

Figure S35: The UV absorption values of PAP at different concentrations and the concentration-dependent change in absorption at 345 nm.

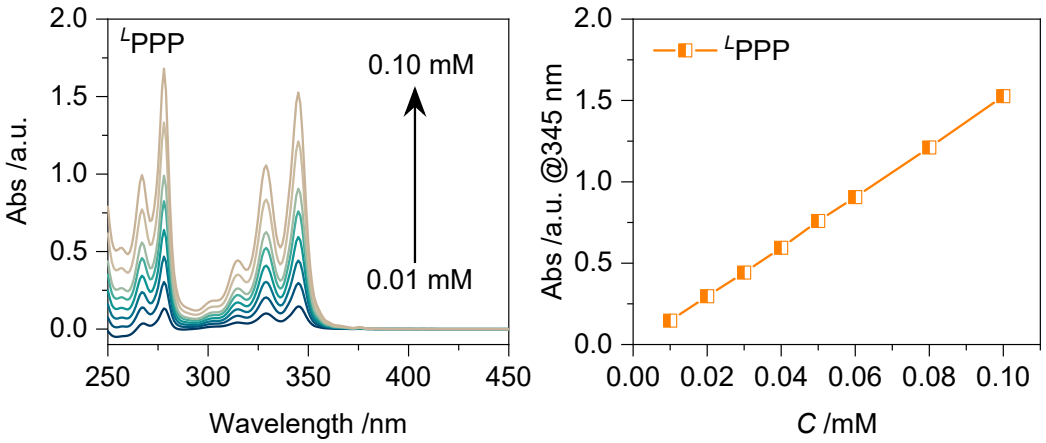

Figure S36: The UV absorption values of PPP at different concentrations and the concentration-dependent change in absorption at 345 nm.

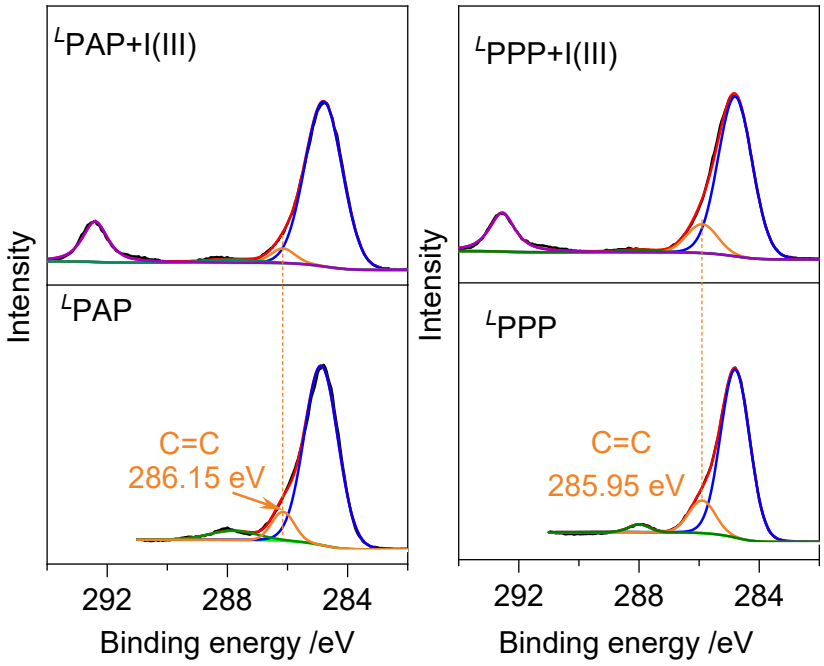

Figure S37: XPS patterns of ^{L}PAP, ^{L}PPP and its halogen bonding complex with the 1:1 ratio

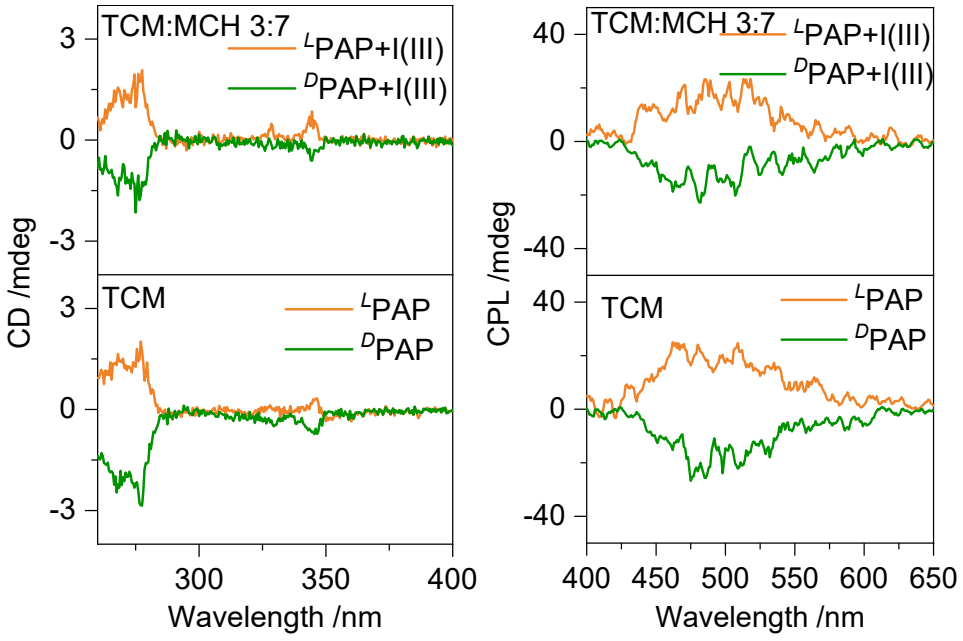

Figure S38: CD and CPL of PAP and PAP+I(III) in the assembly system.

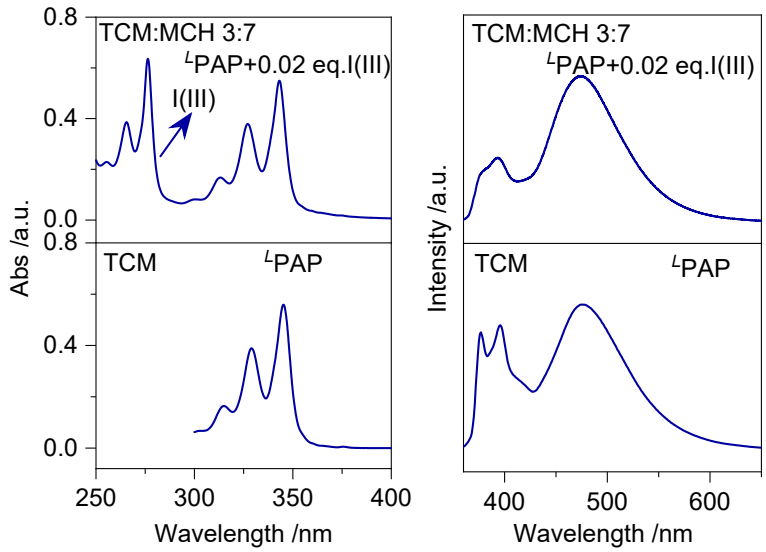

Figure S39: Absorption and fluorescence intensity of PAP and PAP+I(III) in the assembly system.

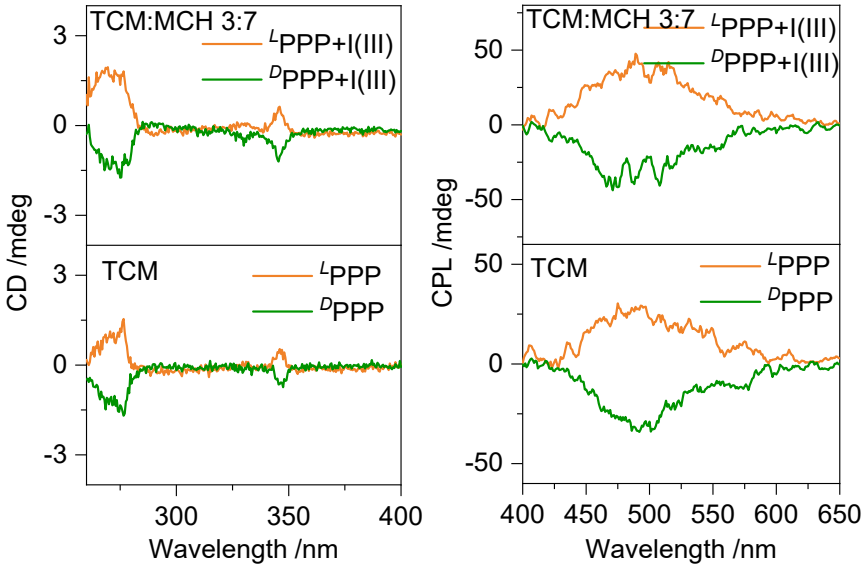

Figure S40: CD and CPL of PPP and PPP+I(III) in the assembly system.

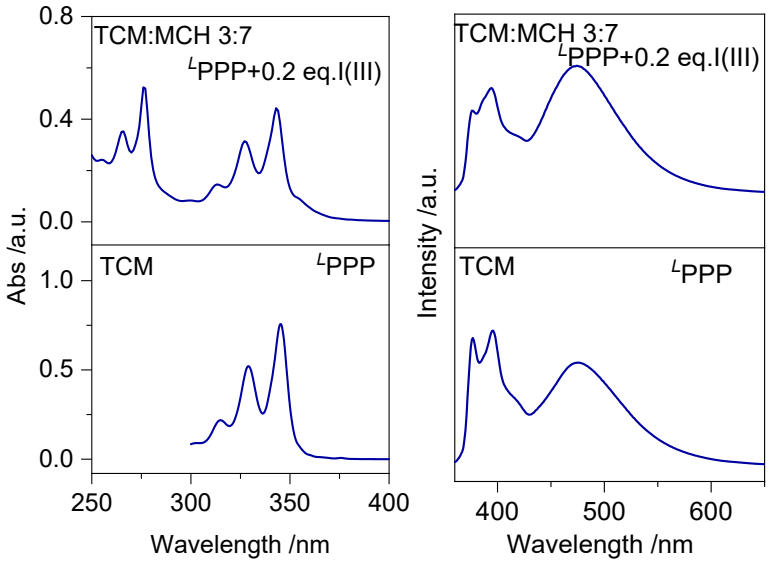

Figure S41: Absorption and fluorescence intensity of PPP and PPP+I(III) in the assembly system.

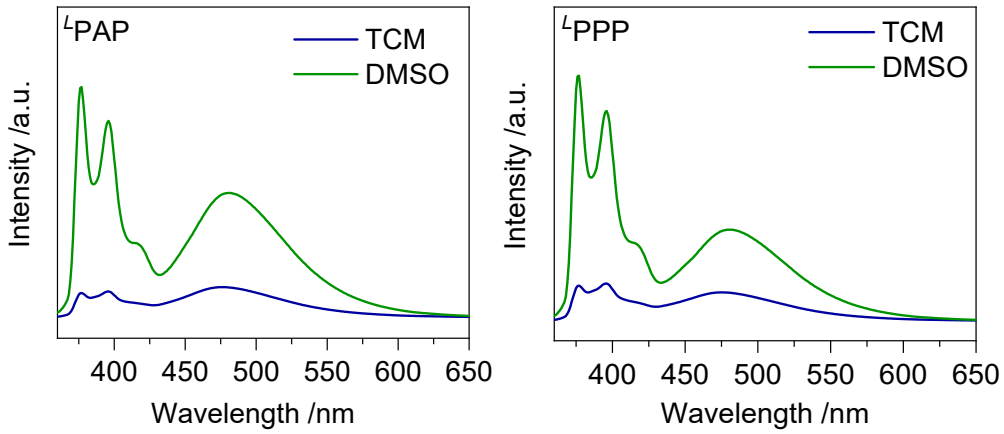

Figure S42: Comparison of the fluorescence intensity of PAP and PPP in TCM and DMSO.

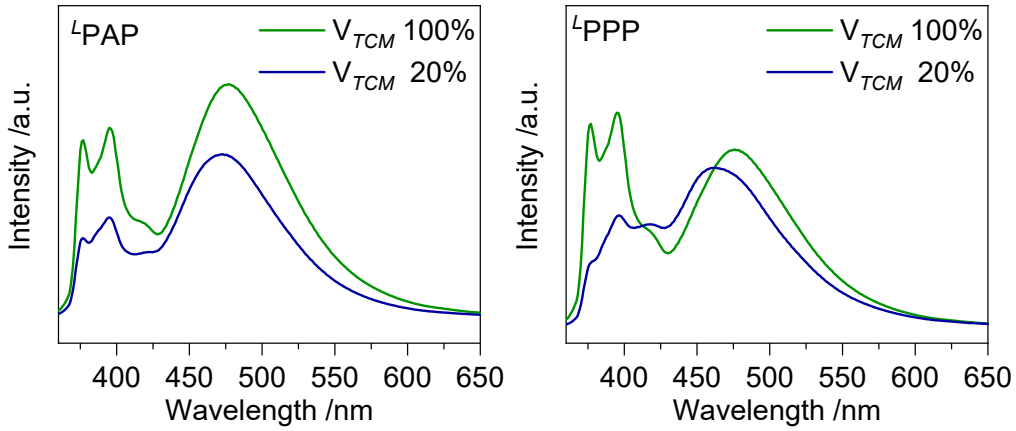

Figure S43: Aggregation-caused quenching (ACQ) occurs during the assembly process

V. Synthesis and characterization

(a) Synthesis of PAP

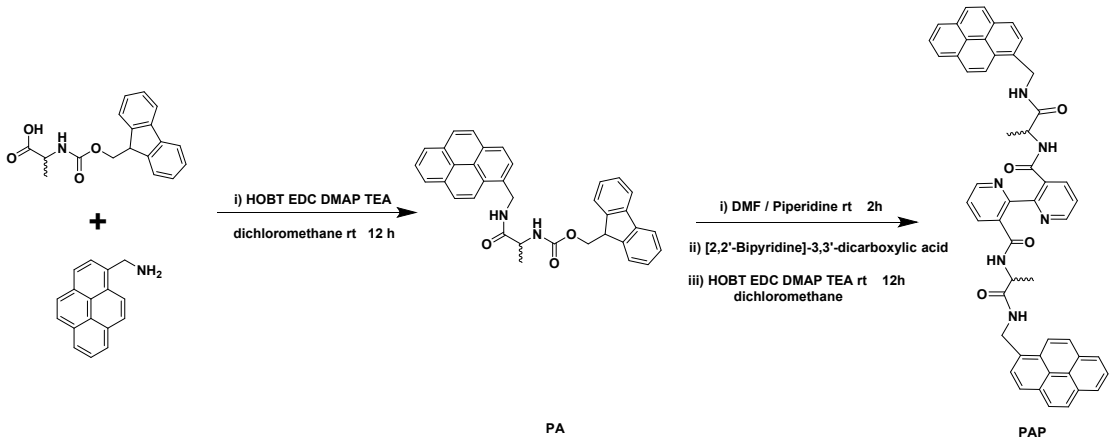

Combine 622 mg of Fmoc-Ala-OH (2 mmol) and 500 mg of Pyren-1-ylmethanamine hydrochloride (1.86 mmol) in a 500 mL round-bottom flask. Add 250 mL of dichloromethane and stir until dissolved. Then, add 200 mg of 1-Hydroxybenzotriazole (HOBT), 300 mg of 1-Ethyl-3-(3-dimethylaminopropyl) carbodiimide (EDC), 20 mg of 4-Dimethylaminopyridine (DMAP), and 0.5 mL of trimethylamine (TEA). Stir the reaction mixture for 12 hours. After the reaction, transfer the mixture to a separatory funnel and extract it three times with dichloromethane. Dry the combined organic extracts with anhydrous sodium sulfate, filter, and then concentrate under reduced pressure. The crude product is purified by column chromatography on silica gel to yield PA. Yield: 838.74 mg, 80%. Take the obtained white powder and place it in a 250 mL round-bottom flask. Add 40 mL of N, N-Dimethylformamide (DMF) and 10 mL of piperidine, and let it react for two hours. Monitor the reaction progress using thin-layer chromatography (TLC). After completion of the reaction, transfer the mixture to a separatory funnel and extract it with dichloromethane (CH_2Cl_2) ten times. Under reduced pressure, concentrate to obtain a yellowish-white powder. Transfer 1g PA into a 500 mL round-bottom flask, add 200 mL of dichloromethane (CH_2Cl_2), and then add 200 mg of [2,2'-Bipyridine]-3,3'-dicarboxylic acid, 130 mg of HOBT, 12 mg of DMAP, and 200 mg of EDC. Let the reaction proceed for 12 hours. After completion of the

reaction, transfer the mixture to a separatory funnel and extract it three times with dichloromethane. Concentrate the combined organic extracts under reduced pressure and purify by silica gel column chromatography to obtain the final product PAP. Yield: 487.2 mg, 30.6%, melting point, 212.6℃, ^{L}PAP, $[\alpha]^{25}_{D}$ =21.93 (5.0 g/ml, DMSO). ^{1}H NMR (400 MHz, DMSO-d_6) δ 8.65 (d, J = 7.6 Hz, 2H), 8.58 – 8.46 (m, 4H), 8.37 – 7.93 (m, 20H), 7.41 (dd, J = 7.8, 4.8 Hz, 2H), 5.07 – 4.91 (m, 4H), 4.40 (p, J = 7.1 Hz, 2H), 1.11 (d, J = 7.0 Hz, 6H). ^{13}C NMR (101 MHz, DMSO) δ 172.03, 167.49, 156.30, 149.61, 136.78, 133.07, 132.27, 131.26, 130.76, 130.51, 128.40, 127.98, 127.84, 127.46, 126.71, 126.66, 125.70, 125.62, 125.21, 124.46, 124.37, 123.53, 123.23, 49.22, 40.89, 40.62, 40.42, 40.21, 40.00, 39.79, 39.58, 39.37, 18.53. HRMS (ESI) m/z [M+H]+, calcd for $C_{52}H_{40}N_6O_4$, 813.3111; found 813.3414.

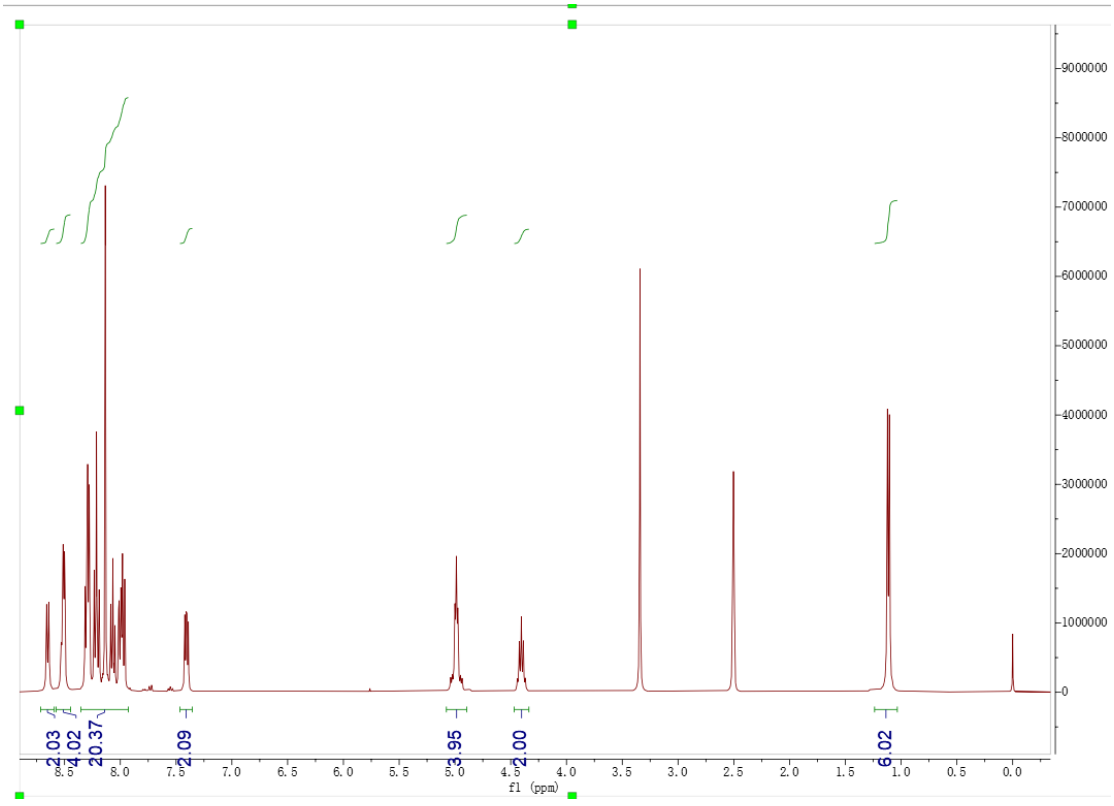

Figure S44: ^{1}H NMR spectrum of ^{L}PAP.

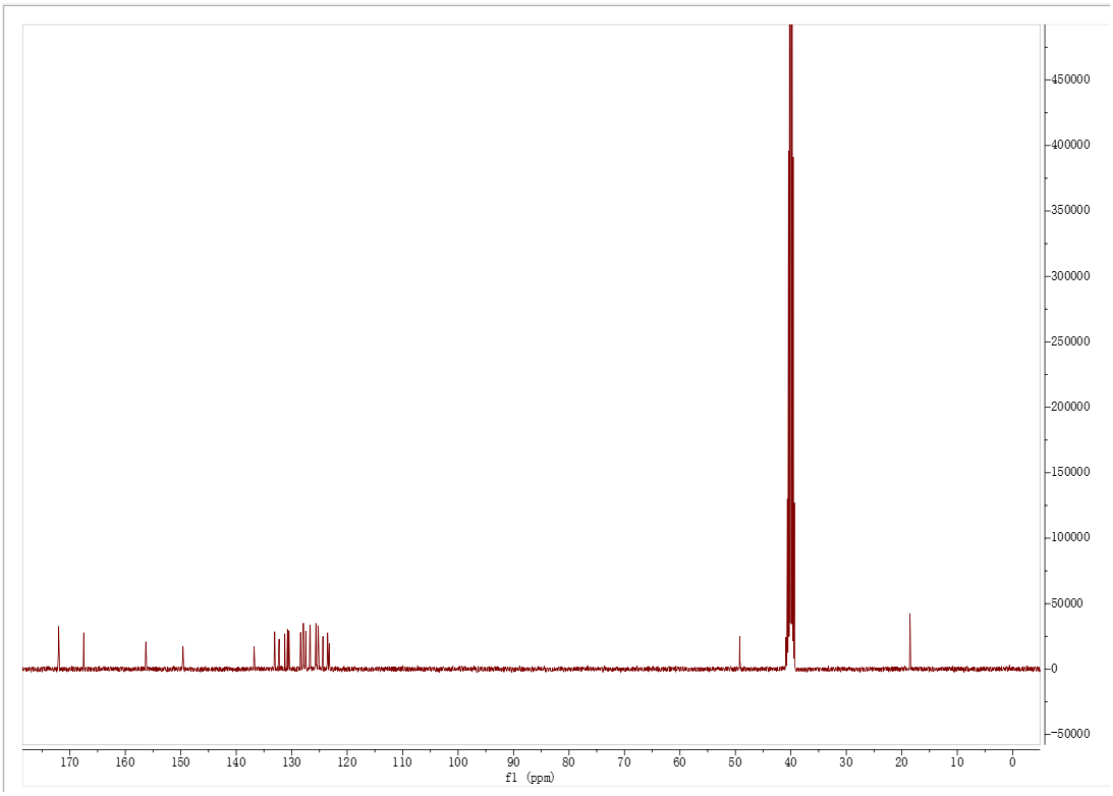

Figure S45: ^{13}C NMR spectrum of ^{L}PAP.

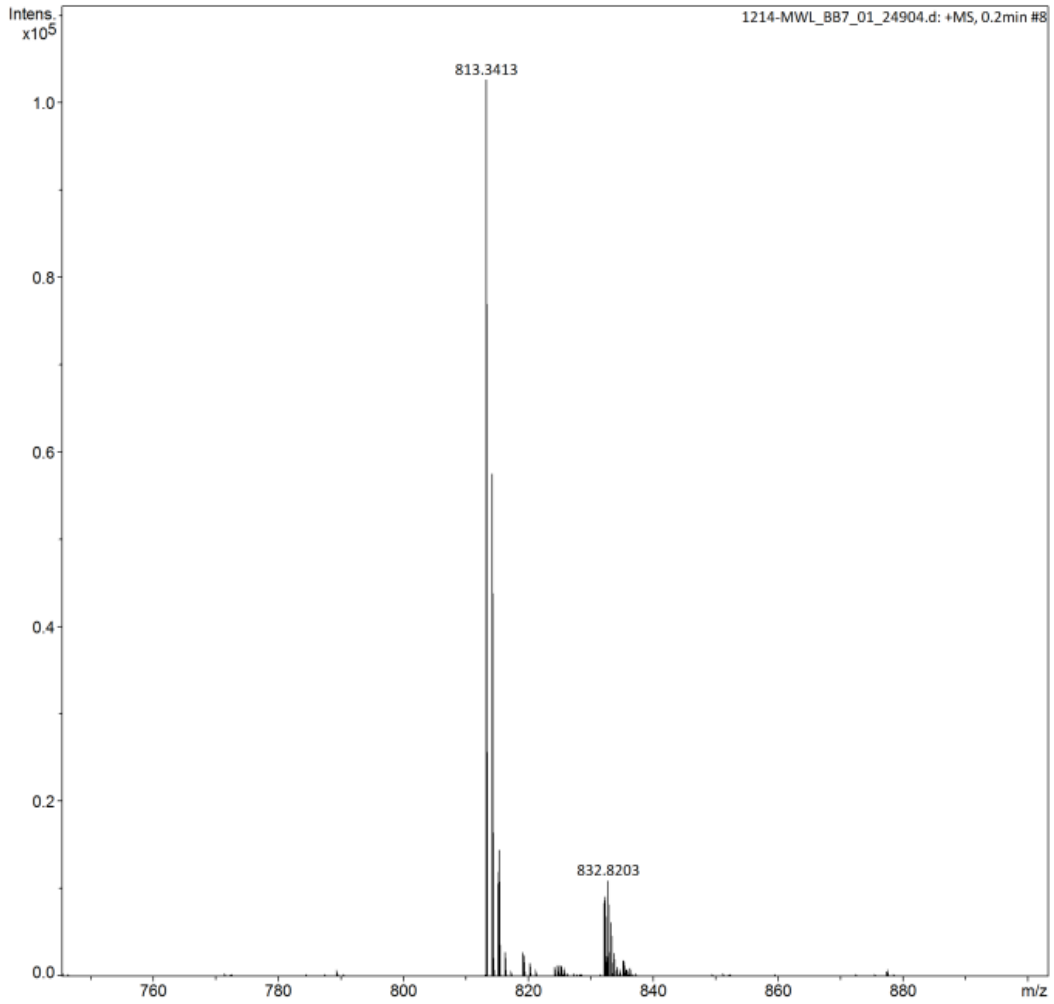

Figure S46: HRMS spectrum of ^{L}PAP.

^{L}PA:^{1}H NMR (400 MHz, DMSO-d6) δ 8.61 (t, J = 5.7 Hz, 1H), 8.35 (d, J = 9.3 Hz, 1H), 8.32 – 8.11 (m, 6H), 8.11 – 8.03 (m, 2H), 7.89 (d, J = 7.5 Hz, 2H), 7.73 (d, J = 7.5 Hz, 2H), 7.63 (d, J = 7.6 Hz, 1H), 7.46 – 7.36 (m, 2H), 7.31 (tdd, J = 7.5, 2.9, 1.2 Hz, 2H), 5.11 – 4.95 (m, 2H), 4.31 – 4.09 (m, 4H), 1.28 (d, J = 7.2 Hz, 3H). ^{13}C NMR (101 MHz, DMSO) δ 171.93, 155.14, 143.30, 143.17, 140.09, 132.19, 130.17, 129.67, 129.45, 127.40, 127.01, 126.86, 126.77, 126.45, 126.39, 125.78, 125.63, 124.71, 124.62, 124.53, 124.09, 123.39, 123.28, 122.57, 119.49, 65.02, 49.64, 46.00, 39.50, 39.35, 39.29, 39.09, 38.88, 38.67, 38.46, 38.25, 17.67. HRMS (ESI) m/z [M+H]+, calcd for $C_{35}H_{28}N_2O_3$, 525.2133; found 525.2134.

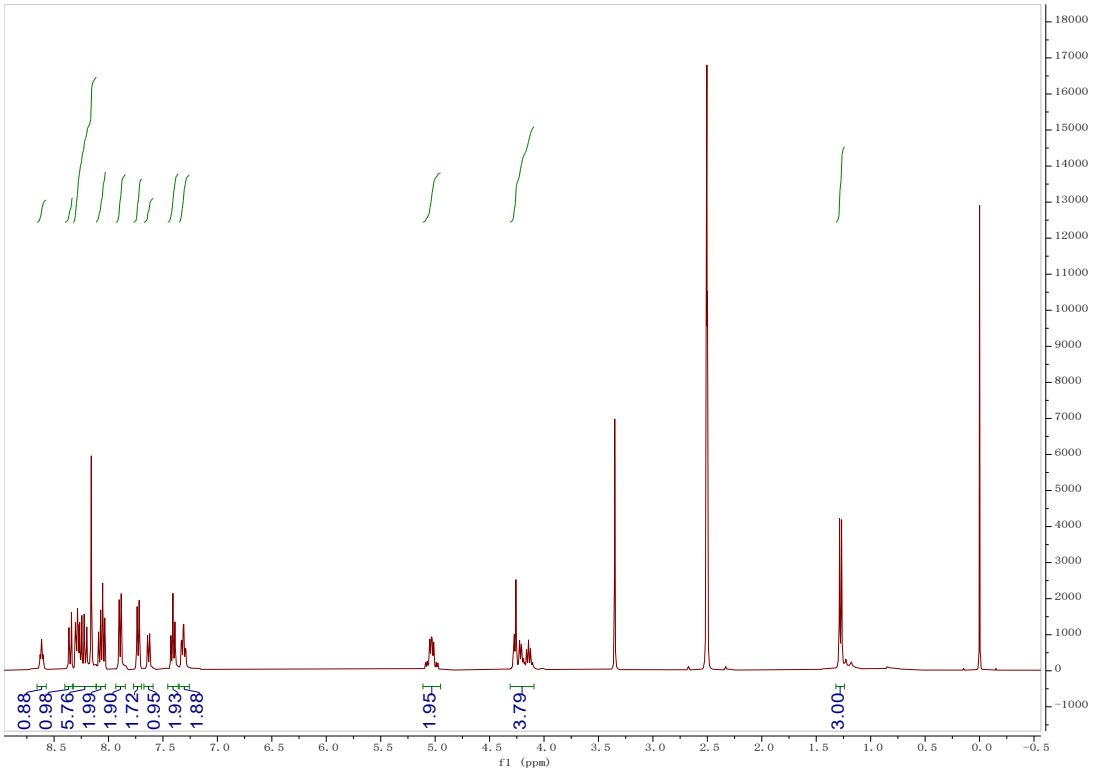

Figure S47: ^{1}H NMR spectrum of ^{L}PA.

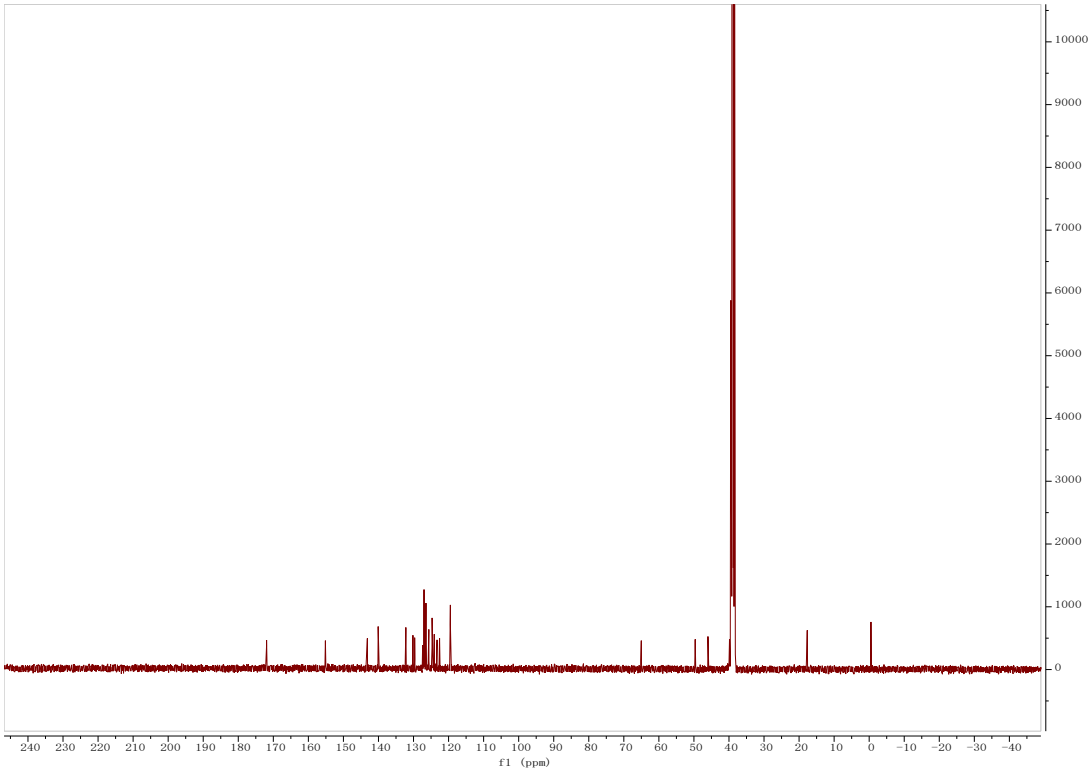

Figure S48: ^{13}C NMR spectrum of ^{L}PA.

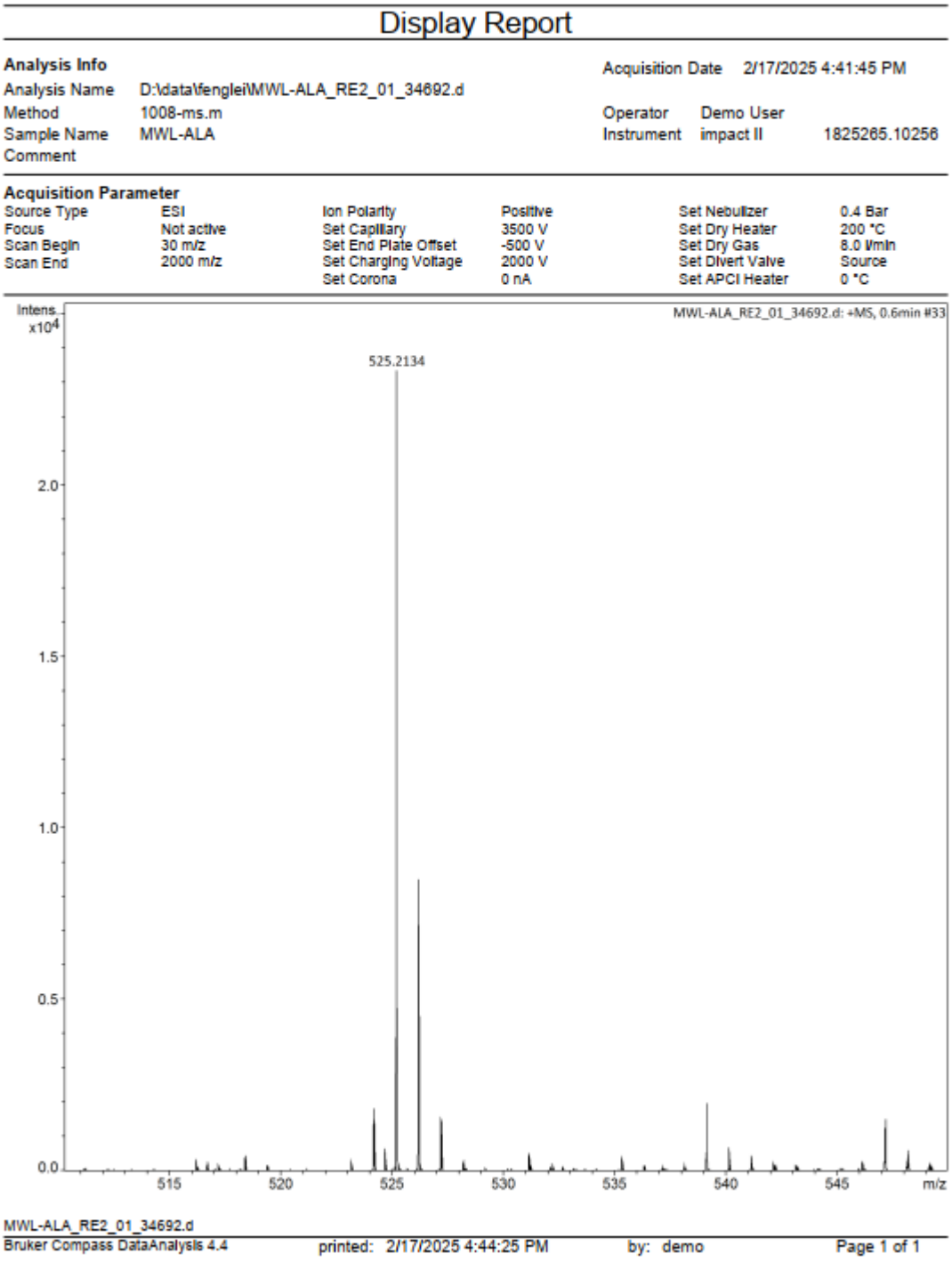

Figure S49: HRMS spectrum of ^{L}PA.

(b) Synthesis of PPP

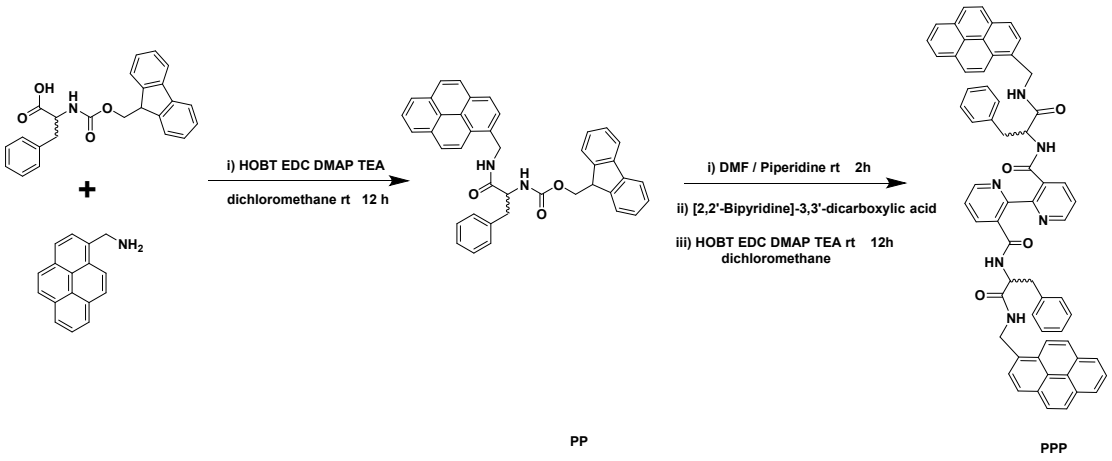

Combine 775 mg of Fmoc-Phenylalanine (2 mmol) and 500 mg of Pyren-1-ylmethanamine hydrochloride (1.86 mmol) in a 500 mL round-bottom flask. Add 250 mL of dichloromethane and stir until dissolved. Then, add 200 mg of 1-Hydroxybenzotriazole (HOBT), 300 mg of 1-Ethyl-3-(3-dimethylaminopropyl) carbodiimide (EDC), 20 mg of 4-Dimethylaminopyridine (DMAP), and 0.5 mL of trimethylamine (TEA). Stir the reaction mixture for 12 hours. After the reaction, transfer the mixture to a separatory funnel and extract it three times with dichloromethane. Dry the combined organic extracts with anhydrous sodium sulfate, filter, and then concentrate under reduced pressure. The crude product is purified by column chromatography on silica gel to yield PP. Yield: 840.34 mg, 70%. Take the obtained white powder and place it in a 250 mL round-bottom flask. Add 40 mL of N, N-Dimethylformamide (DMF) and 10 mL of piperidine, and let it react for two hours. Monitor the reaction progress using thin-layer chromatography (TLC). After completion of the reaction, transfer the mixture to a separatory funnel and extract it with dichloromethane (CH_2Cl_2) ten times. Under reduced pressure, concentrate to obtain a yellowish-white powder. Transfer 1.2g PP into a 500 mL round-bottom flask, add 200 mL of dichloromethane (CH_2Cl_2), and then add 200 mg of [2,2'-Bipyridine]-3,3'-dicarboxylic acid, 130 mg of HOBT, 12 mg of DMAP, and 200 mg of EDC. Let the reaction proceed for 12 hours. After completion of the reaction, transfer the mixture to a separatory funnel and extract it three times with dichloromethane. Concentrate the combined organic extracts under reduced pressure and purify by silica gel column

chromatography to obtain the final product PPP. Yield: 386.60 mg, 20%, ^{L}PPP, melting point, 220.2℃，$[\alpha]^{25}_{D}$ =35.13 (5.0 g/ml, DMSO).

^{1}H NMR (400 MHz, DMSO-d_6) δ 8.81 (d, J = 8.2 Hz, 2H), 8.61 (t, J = 5.8 Hz, 2H), 8.39 – 8.24 (m, 8H), 8.23 – 8.03 (m, 11H), 7.81 (d, J = 7.9 Hz, 2H), 7.72 (dd, J = 7.8, 1.7 Hz, 2H), 7.30 (dd, J = 7.8, 4.8 Hz, 2H), 7.20 – 7.06 (m, 10H), 4.97 (qd, J = 15.3, 5.7 Hz, 4H), 4.64 (td, J = 8.5, 5.9 Hz, 2H), 2.92 (dd, J = 13.8, 5.8 Hz, 2H), 2.73 (dd, J = 13.7, 8.8 Hz, 2H). ^{13}C NMR (101 MHz, DMSO-d_6) δ 170.87, 167.69, 156.22, 149.45, 137.89, 136.46, 132.84, 132.09, 131.25, 130.76, 130.49, 129.46, 128.56, 128.39, 127.98, 127.84, 127.45, 126.70, 126.66, 125.69, 125.62, 125.18, 124.43, 124.37, 123.56, 123.06, 54.95, 40.95, 38.0 2. HRMS (ESI) m/z $[M+H]^{+}$, calcd for $C_{64}H_{48}N_6O_4$, 965.3737; found 965.3660.

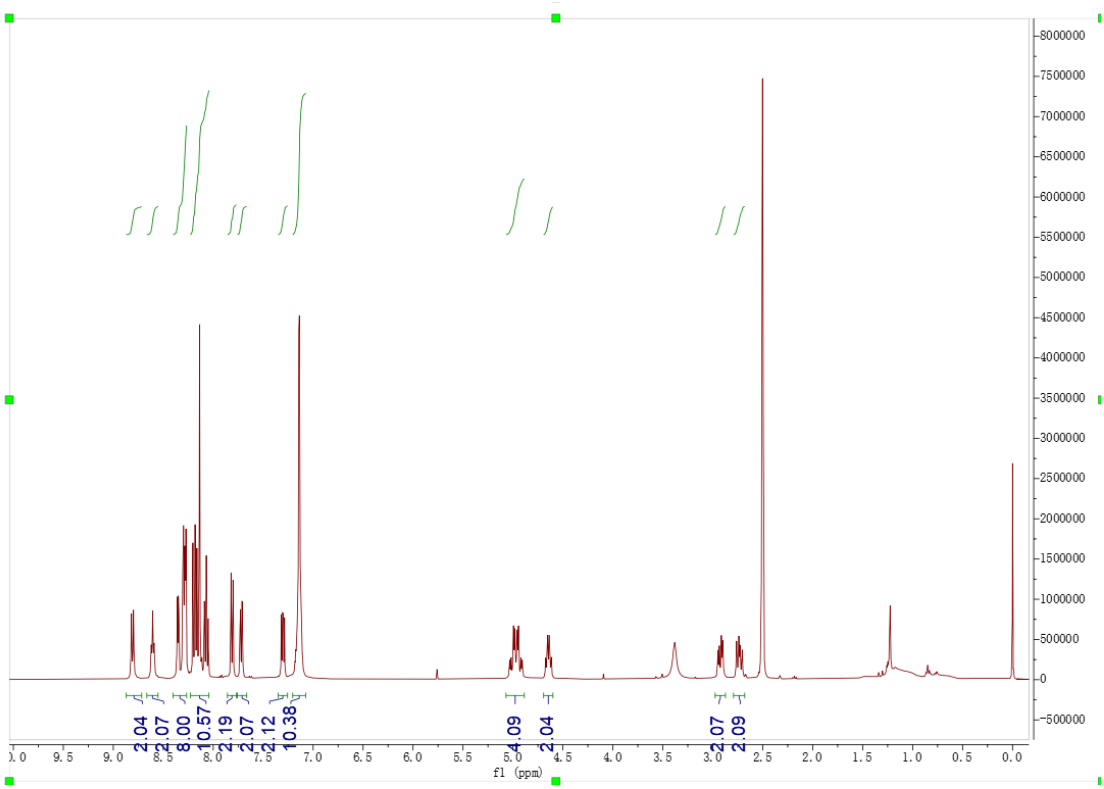

Figure S50: ^{1}H NMR spectrum of ^{L}PPP.

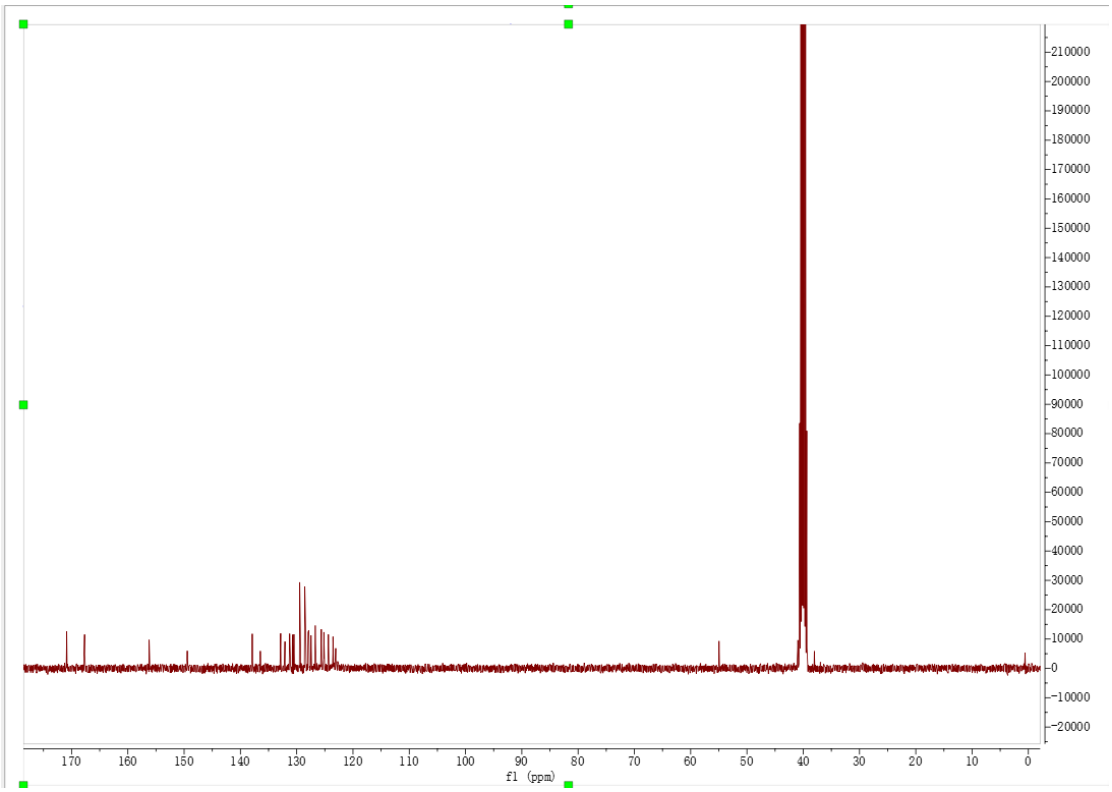

Figure S51: ^{13}C NMR spectrum of ^{L}PPP.

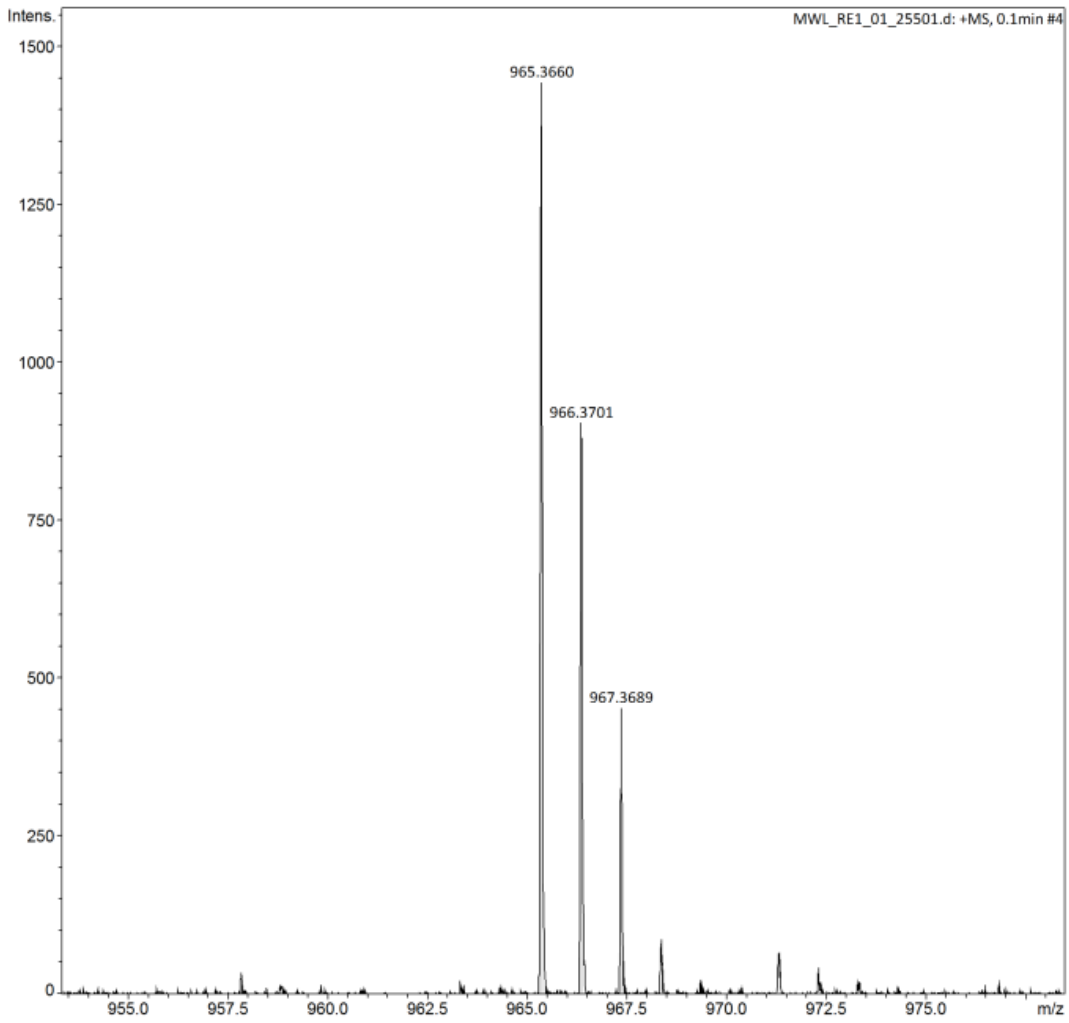

Figure S52: HRMS spectrum of ^{L}PPP.

^{L}PP: ^{1}H NMR (400 MHz, DMSO-d6) δ 8.78 (t, J = 5.6 Hz, 1H), 8.36 (dd, J = 9.4, 4.8 Hz, 1H), 8.31 – 8.16 (m, 6H), 8.07 (t, J = 7.6 Hz, 1H), 7.96 (d, J = 7.8 Hz, 1H), 7.88 (dd, J = 7.6, 2.7 Hz, 2H), 7.77 (d, J = 8.6 Hz, 1H), 7.65 (dd, J = 12.9, 7.5 Hz, 2H), 7.41 (dp, J = 10.6, 3.6, 2.9 Hz, 2H), 7.33 – 7.15 (m, 8H), 5.10 – 4.99 (m, 2H), 4.35 (td, J = 9.8, 9.2, 4.7 Hz, 1H), 4.23 – 4.04 (m, 3H), 3.03 (dd, J = 13.6, 4.8 Hz, 1H), 2.88 (dd, J = 13.6, 10.2 Hz, 1H). ^{13}C NMR (101 MHz, DMSO) δ 170.82, 155.23, 143.16, 143.12, 140.04, 137.46, 136.80, 131.99, 130.16, 129.67, 129.48, 128.63, 128.32, 127.44, 127.00, 126.89, 126.77, 126.68, 126.42, 125.89, 125.63, 124.77, 124.67, 124.62, 124.54, 124.09, 123.39, 123.28, 122.58, 120.79, 119.47, 119.43, 65.06, 55.79, 45.91,

39.50, 39.29, 39.09, 38.88, 38.67, 38.46, 38.25, 37.03. HRMS (ESI) m/z $[M+Na]^+$, calcd for $C_{41}H_{32}N_2O_3Na$, 623.2413; found 623.2303.

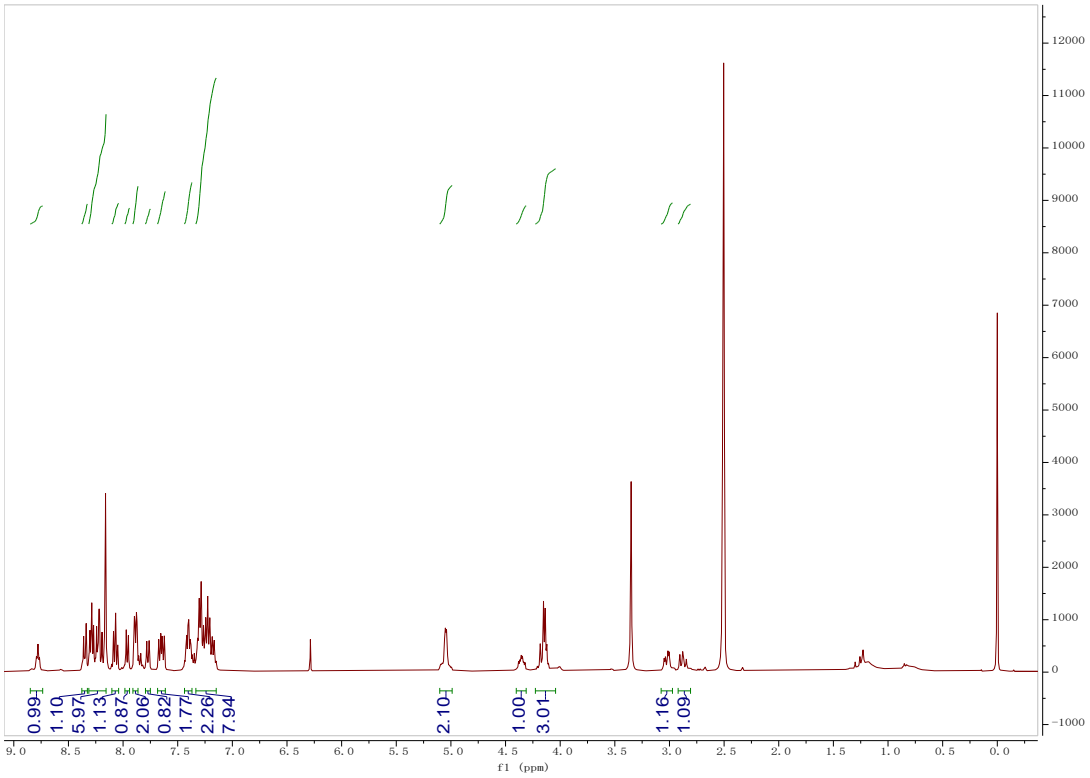

Figure S53: ^{1}H NMR spectrum of ^{L}PP.

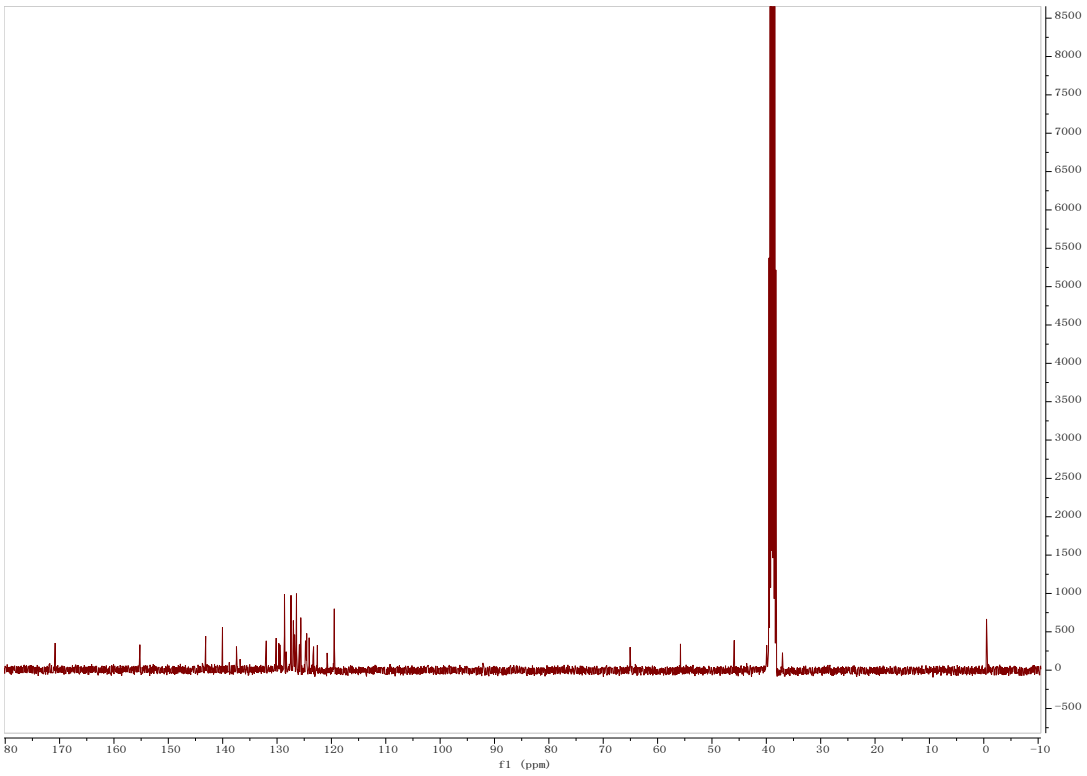

Figure S54: ^{13}C NMR spectrum of ^{L}PP.

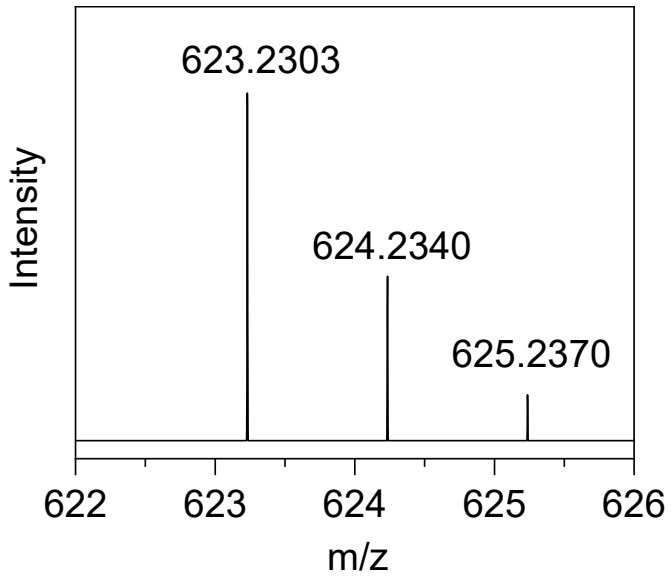

Figure S55: HRMS spectrum of ^{L}PP.

(c) Synthesis of I(III)

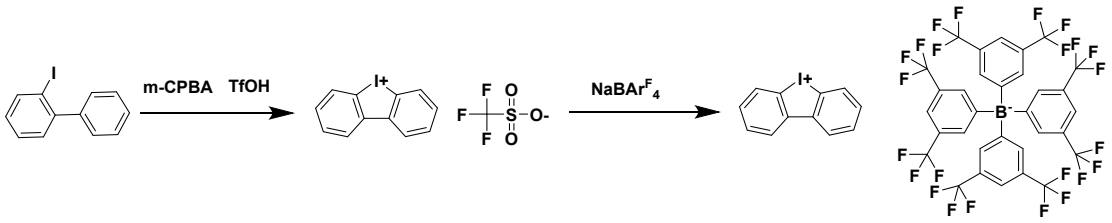

The preparation of halogen bonding donor using the method published by S. Wen and S. M. Huber et. al.[1-2]

To a stirred solution of 2-iodobiphenyl (1.1 g, 3.93 mmol) in anhydrous CH_2Cl_2 (10 mL), m-CPBA (1.02 g, 5.89 mmol) and TfOH (1.04 mL, 11.78 mmol) were added. The solution was stirred for 1 hour at room temperature. CH_2Cl_2 was removed by rotary evaporation, and then 15 mL of Et_2O (diethyl ether) was added. The mixture was stirred for 20 minutes and then filtered. The collected solid was washed with Et_2O (three times) and dried under vacuum to yield a white solid. 1.07 g of I(III)·$^-$OTf (2.5 mmol) and 2.17 g of sodium NaBAr$^F_4$ (2.45 mmol, 0.98 equivalents) were suspended in 50 mL of chloroform and stirred for 4 days at room temperature. The precipitated NaOTf was filtered off. The remaining solution was cooled in the freezer, decanted to remove any remaining residue. After vacuum concentration, the solution was refrigerated, resulting in the formation of yellow crystals. These crystals were collected, dried under vacuum to yield I(III)·BAr$^F_4$. Yield: 60%. ^{1}H NMR (400 MHz, Chloroform-*d*) δ 8.10 (dd, *J* = 7.9, 1.5 Hz, 2H), 7.82 (t, *J* = 7.6 Hz, 2H), 7.79 – 7.67 (m, 9H), 7.64 – 7.57 (m, 2H), 7.49 (s, 4H). HRMS m/z(+) $[M]^+$, calcd for 278.9665; found, 278.9678.

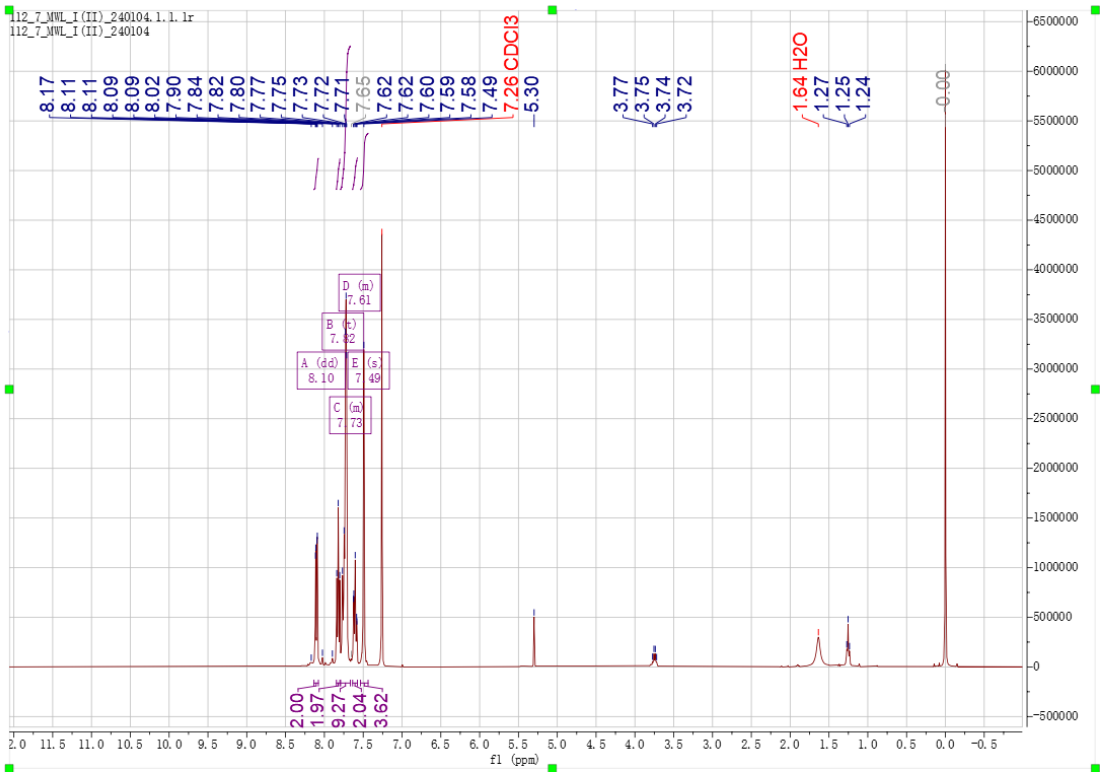

Figure S56: ^{1}H NMR spectrum of I(III)·BAr$^{F}_{4}$.

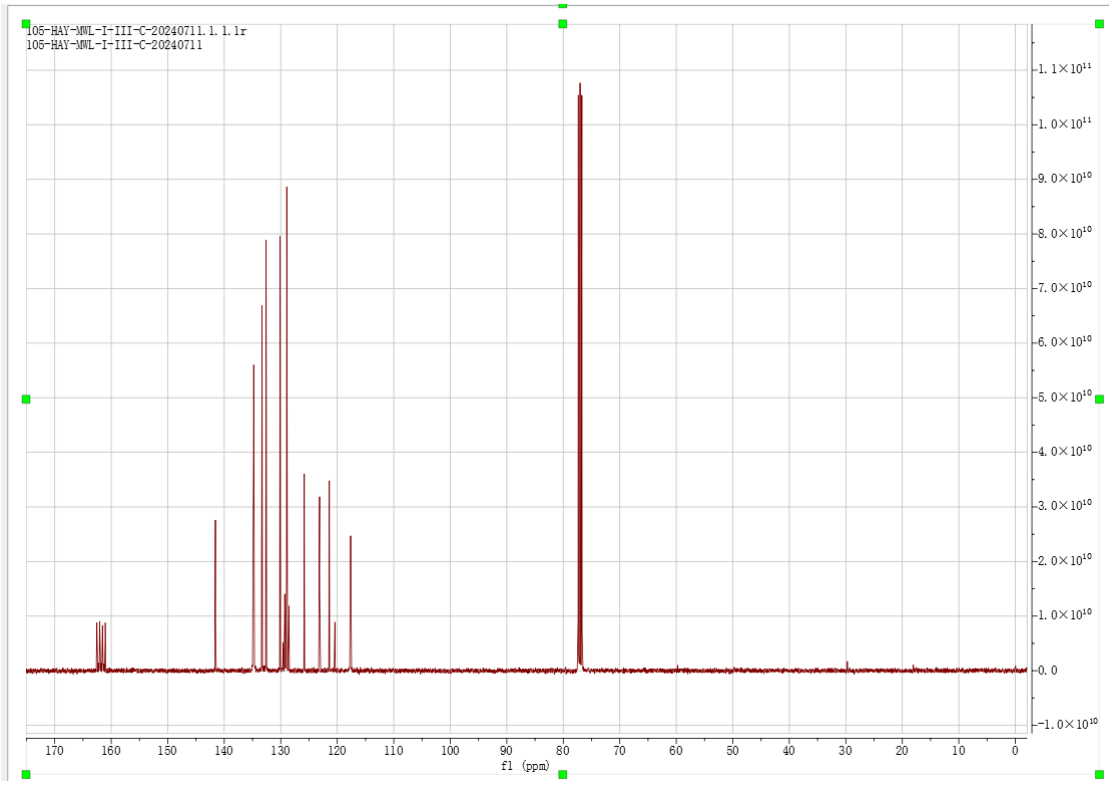

Figure S57: ^{13}C NMR spectrum of I(III)·BAr$^{F}_{4}$.

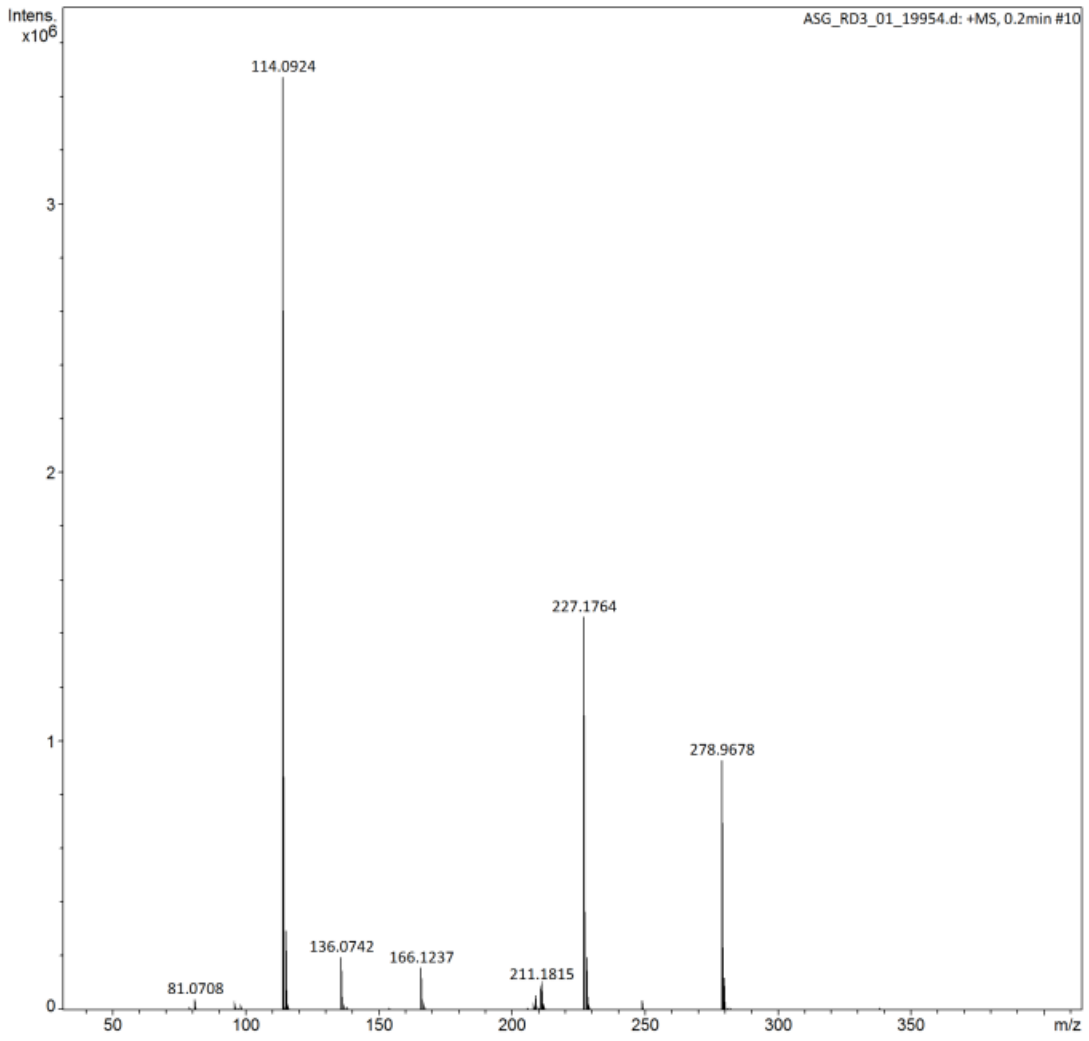

Figure S58: HRMS spectrum of I(III)·BAr^F_4.

[1] Y. Wu, X. Peng, B. Luo, F. Wu, B. Liu, F. Song, P. Huang, S. Wen, *Org. Biomol. Chem.* **2014**, *12*, 9777-9780.

[2] F. Heinen, E. Engelage, C. J. Cramer, S. M. Huber, *J. Am. Chem. Soc.* **2020**, *142*, 8633-8640.